GAS ABSORPTION IN PACKED COLUMN

KAKUSABURO ONDA

Department of Chemical Engineering

(Received October 25, 1972)

CONTENTS

1. Introduction

In the removal of vapor phase impurities from gas stream or gas purification, the absorption process is most commonly employed in industrial purposes. It involves the mass transfer from the gas to the liquid phase through the interface. The absorbed material may dissolve physically in the liquid phase or react chemically with solvent.

The packed column is the most common unit employed in diffusional processes of absorption, desorption, scrubbing, distillation, extraction and so on. To design a packed column, it is necessary to obtain a knowledge of the individual mass transfer coefficients, k_G and k_L, as well as the interfacial area per unit volume of packed column. Also, the solubility of gases into the liquid is of important factor determing the driving force, and physico-chemical properties of gas and liquid are required to predict k_G and k_L. Chemical reactions of the solute with the solvent are, of cource, in significance with the diffusion process simultaneously.

This paper concerns the various and necessary results to design packed columns for the gas absorption, which have been investigated in our laboratory, and author expresses heartily thanks for many investigators whose names are listed in each literature.

2. Vapor-Liquid Equilibria

2.1. Vapor pressure of carbon monoxide over copper liquor

Carbon monoxide removal was an important step in the purification of the ammonia-synthesis gas produced by the partial oxidation of hydrocarbons, the water-gas reaction, or steam hydrocabon reforming. However, in this process small quantities of residual carbon monoxide should be removed completely to avoide the poisoning of the catalyst.

Onda *et al.*[1] started an investigations on the copper liquor in 1950, at that time since the cuprammonium carbonate or formate solution had been used as the only absorbent for CO removal processes. However, the mechanism of the absorption of CO by copper liquors was not known with certainty, though it was generally accepted that the quantity of CO absorbed approaches one mole of CO per mole of cuprous ion, indicating that the compound formed contains both components with the relation of 1 to 1.

Onda *et al.*[2] found that the equilibria of CO and copper liquor vary with the concentration of ammonia, and the equilibria could be presented with the "copper to ammonia ratio", N, defined as the ratio of total NH_3 to the effective cuprous concentration. By assuming the structure of cuprammonium complex, the equilibrium constant was estimated, and whether the

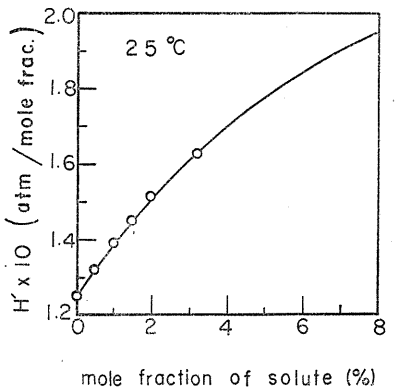

FIG. 1. Henry's constant of CO for copper liquor.

resultant value is constant or not with variation of the partial pressure of CO was discussed[4]. Furthermore, such reaction mechanisms were confirmed from the electric conductivity of copper liquor[3]. On the other hand, to determine the equilibrium constant, Henry's law constant for the gas which reacts with a component in solution was predicted by considering the various salts to be constituent of the copper liquors[1]. Fig. 1 shows the plot of H/H_w versus the mole fraction of solute.

2.2. Solubilities of methane in liquid hydrocarbons[5][6]

The removal of hydrocarbon vapors from gas streams by absorption in liquid oils has been an important part of a great many industrial processes with an advancement of modern petrochemicals. In our laboratory, it had been studied on the solubilities of methane in various organic solvents[5].

In the first place, solubilities of CH_4 in kerosene had been measured at temperature ranging from 0 to 30°C under pressures of 60 atm. Experimental results are shown in Fig. 2, which is plotted as the fugacity of methane in gas phase versus the mole fraction in liquid phase. The effect of temperature on Henry's constant was expressed by

$$\ln H' = (\Delta H_s/RT) + A \qquad (1)$$

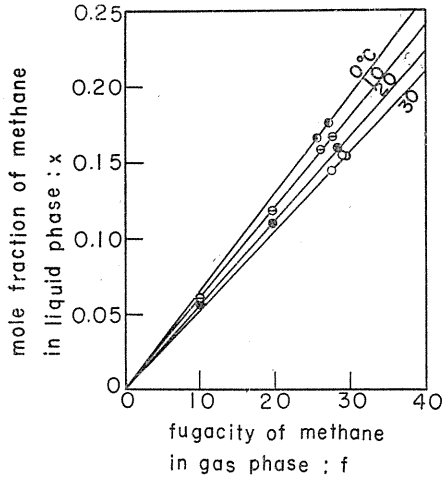

FIG. 2. Solubility of CH_4 in kerosen.

where ΔH_s is the enthalpy of solution, that is, the heat of solution: A is a constant. As a result, Onda *et al.*[6] suggested that the heat of solution could be estimated from the solubility data.

In sucession, as shown in Fig. 3, solubilities of methane in *n*-hexane, *n*-heptane, *n*-octane, *n*-dodecane, benzene, toluene, and xylene oils were measured under atmospheric pressure[6]. It was found that the relation between H' and the temperature for each system shows the same linearlity as that for CH_4-kerosene system and from the slope of each line, the heat of solution could be calculated. For oils of seven kinds of aforementioned hydrocarbon, values of ΔH_s took a definite value to be -0.862 kcal/mol regardless of aromatic or paraffinic compound.

To consider a signigicance of the constant A in Eq. (1), Onda *et al.*[6] had assumed a mechanism of solution that a gaseous solute molecule is introduce into the cavity of suitable size to accomodate the solute molecule,

$$(\text{Solute})_G + \text{Cavity} \rightleftarrows (\text{Solute})_L \qquad (2)$$

The equilibrium constant for Eq. (2) is expressed by

$$K = \frac{C_s}{C_l a_s} = x_s \Big/ \left(\frac{C_l}{C_s + C_{so}}\right) \cdot a_s \qquad (3)$$

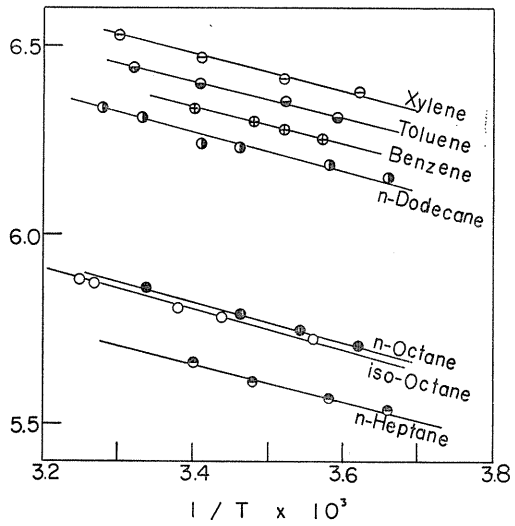

FIG. 3. Solubility of CH_4 in various hydrocarbon oils.

where a_s is the activity of solute molecule in gas phase: C_l and C_s is the molarity of cavity and solute gas in the solvent, respectively: C_{so} is the molarity of solvent. Defining m as the number of average free volume, v_{so}^f, necessary to create a cavity in the solvent,

$$C_l/(C_s+C_{so}) \simeq C_l/C_{so} = 1/m \tag{4}$$

In Eq. (3), by taking a fugacity so as to $a_s=p$, K is expressed by

$$K = mx_s/p \tag{5}$$

where x_s is the mole fraction of solute in liquid; p is the partial pressure of the solute. Then from Henry's law, p/x could be substituted by H'. Furthermore, from a thermodynamical consideration and the assumption that the volume of solute molecule is negligible to the cavity, A is defined by

TABLE 1. Entropy of solution of methane for various organic solvents

Solvent	A	m	r(Å)	ΔS (cal/mol·°K)
n-heptane	7.12	70.3	5.8	−5.70
n-octane	7.28	67.3	5.5	−6.10
iso-octane	7.27	67.1	5.4	−6.10
n-dodecane	7.74	60.8	5.6	−7.20
benzene	7.80	60.4	5.2	−7.35
toluene	7.86	59.7	5.2	−7.52
xylene	7.93	59.3	4.9	−7.65

$$A = \ln \frac{mx_s}{x_{so} + mx_s} - \frac{x_{so}(m-1)}{x_{so} + mx_s} - \ln \frac{v_{so}^f}{V_{sm}^G} \tag{6}$$

where V_{sm}^G is the molecular volume of solute gas.

Hence, using A obtained from the experimental results, m which is the number contributing to the free volume or volume of a cavity and the entropy of solution would be estimated, respectively. These calculated values for the aforementioned systems are shown in Table 1, in which m decreases with an increase of the number of carbon atom irrespective of aromatic or paraffinic compounds. Also as seen in Table 1, the radius of the cavity is constant to be about 5 Å.

2.3. Gas solubility in aqueous salt solutions

Predicting the solubility of gases in aqueous salt solution is indispensable to investigate the mass transfer between gas and liquid phases, especially the gas absorption with chemical reaction.

In general, when both the salt and the nonelectrolyte solute gas concentrations, C_s and C_i, are low, and there is no chemical interaction between solute species, the activity coefficient of nonelectrolyte solute in aqueous salt solution, f_i, is given by

$$\log f_i = k_s C_s + k_i C_i \tag{7}$$

The last term of Eq. (7) can be ignored if k_i which results from the interaction of the nonelectrolyte with itself or C_i is very small. In gas solubility studies, C_i is often small enough to justify ignoring the k_i-term. Experimental measurments of the solubility of a gas in pure solvent and in a salt solution give the activity coefficient of the dissolved gas directly. The gas solute activity is the same in pure solvent and salt solution, then

$$f_i S_i = f_i^\circ S_i^\circ \tag{8}$$

where S_i° and S_i are gas solubility in pure solvent and salt solution, respectively. Thus

$$\log (f_i/f_i^\circ) = \log (S_i^\circ/S_i) = k_s C_s + k_i (S_i - S_i^\circ) \tag{9}$$

and if S_i° and S_i are small, the last term can be ignored

$$\log (f_i/f_i^\circ) = \log (S_i^\circ/S_i) = k_s C_s \tag{10}$$

which is the same form as the well-known empirical Setschnow equation;

$$\log (S_i^\circ/S_i) = K_s C_s \tag{11}$$

Van Krevelen and Hoftijzer[9] have regarded the parameter as the sum of constants which are characteristic of gases, cations and anions as follows

$$K_s = x_g + x_c + x_a \tag{12}$$

Moreover, they have assumed that x_c and x_a are independent of temperature and only x_g is dependent on it, and have proposed that ionic strength I should

be used instead of C_s. As a result, Eq. (11) is represented by

$$\log (S_i^\circ / S_i) = K_s I \qquad (11)'$$

where

$$I = (Z_c^2 C_c + Z_a^2 C_a)/2$$

and Z and C is the ionic valency and the concentration, respectively. In their paper, the ionic strengh is restricted to the range of less than 2 g-ions/l.

Onda *et al.*[7] carried out to measure solubilities of carbon dioxide and ethylene at about 1 atm. and 25°C in a number of aqueous salt solutions whose ionic strength are more than 2 g-ions/l, and showed the method to determine the values of x_g, x_c and x_a.

The results obtained in the experiment are shown in Figs. 4 and 5 in which the ratio of Bunsen coefficients in water α_w to those in aqueous salt solution α versus the ionic strength I are plotted. Straight lines in these figures are calculated by putting Eq. (11) as follows

TABLE 2. Empirical constant in Eq. (12) of the salting-out parameters. (Temperature is shown in parentheses)

gas	x_g	cation	x_c
CO_2 (25)	−0.2277	Li^+	−0.0416
N_2 (25)	−0.1904	Na^+	−0.0183
O_2 (25)	−0.1892	K^+	−0.0362
H_2 (25)	−0.2115	Cs^+	−0.0584
N_2O (25)	−0.2141	Mg^{++}	−0.0568
C_2H_2 (25)	−0.2240	Ca^{++}	−0.0547
H_2S (25)	−0.2551	Ba	−0.0473
SO_2 (25)	−0.3154	Al^{+++}	−0.0726
NH_3 (25)	−0.2394	NH_4^+	−0.0737
C_2H_4 (25)	−0.1951	H^+	−0.1110
He (25)	−0.2220	Rb^+	−0.0449
Ne (25)	−0.2240	Cd^{++}	−0.0062
Ar (25)	−0.1866	Zn^{++}	−0.0590
Kr (25)	−0.1762	Sr^{++}	−0.0445
N_2O (5)	−0.2143	Fe^{++}	−0.0602
N_2O (10)	−0.2156	Co^{++}	−0.0534
N_2O (15)	−0.2118	Ni^{++}	−0.0520
N_2O (20)	−0.2128	Cr^{+++}	−0.0986
N_2O (40)	−0.2179	Mn^{++}	−0.0625
CO_2 (0)	−0.2110	anion	x_a
CO_2 (15)	−0.2222	Cl^-	0.3416
CO_2 (40)	−0.2327	Br^-	0.3310
O_2 (0)	−0.1653	I^-	0.3124
O_2 (15)	−0.1786	SO_4^{--}	0.3446
O_2 (20)	−0.1771	NO_3^-	0.3230
H_2 (5)	−0.2106	CO_3^{--}	0.3754
H_2 (10)	−0.2170	OH^-	0.3875
H_2 (15)	−0.2197	CNS^-	0.2612
H_2 (20)	−0.2132	PO_4^{---}	0.3265
C_2H_2 (15)	−0.2124	SO_3^{--}	0.3275
SO_2 (35)	−0.3122	HSO_3^-	0.3869
C_2H_4 (15)	−0.2003	HS^-	0.3718

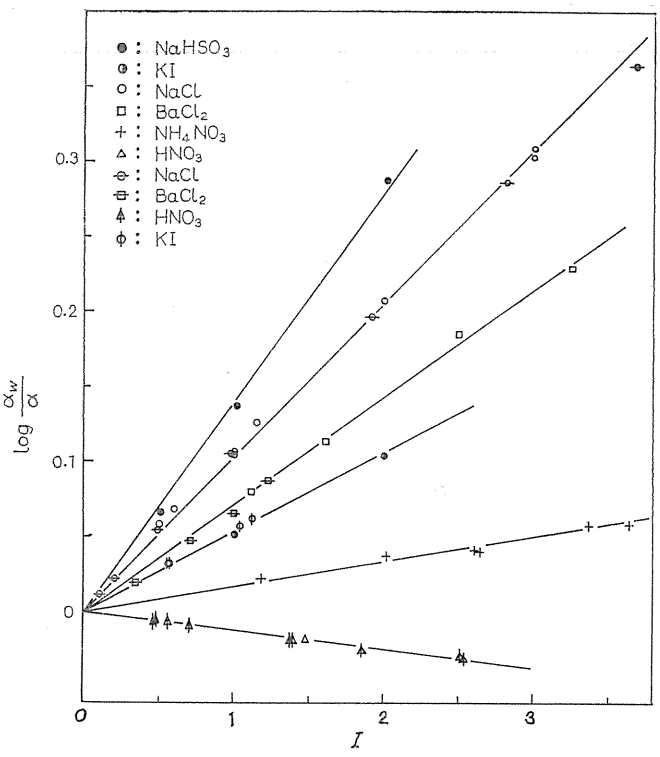

FIG. 4. Experimental results for carbon dioxide at 1 atm. and 25°C.

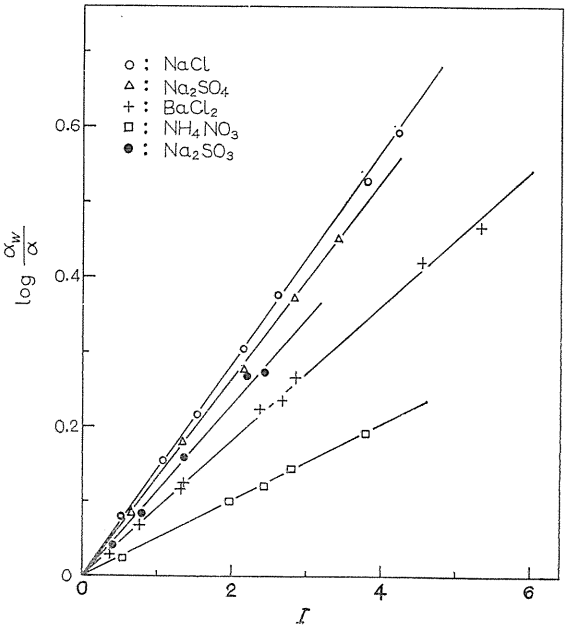

FIG. 5. Experimental results for ethylene at 1 atm. and 25°C.

$$x_g + x_c + x_a = \log(\alpha_w/\alpha)/I \tag{13}$$

As shown in Fig. 4, plots of α_w/α vs. I scatter a little from the straight line. The average values of the right side of Eq. (13) are determined by the least square method.

The calculated results of x_g, x_c and x_a are shown in Table 2. With these calculated salting-out parameters, solubilities of gas in aqueous salt solutions could be predicted within the standard deviation 0.052.

The solubilities of gases in aqueous solutions of mixed salts had been also measured at 1 atm. and 25°C with carbon dioxide, ethylene and acetylene for aqueous solution of two or three mixed salt[8]. From the experimental results, it is approximately possible to establish an additive rule for the salting-out parameters. From this point of view, the solubilities for mixed salts solutions are predicted from the method mentioned above and the standard deviation is 0.024 for overall gas systems, which is smaller than that of van Krevelen, and many data are also added which are not listed in the literature mentioned above.

3. Physico-Chemical Properties

3.1. Density and viscosity of copper liquors[10]

Accurate values of density and viscosity of the copper liquor used in the absorption of carbon monoxide as described in Chap. 2.1, are the basic data not only to design a CO-absorber, but also to make an absorption mechanism or equilibrium clear. Due to the complexity of copper liquor composition and the difficulty of the measurement, however, these values are very few in literatures.

Density

Since the composition of copper liquor is rapidly changeable with oxygen in

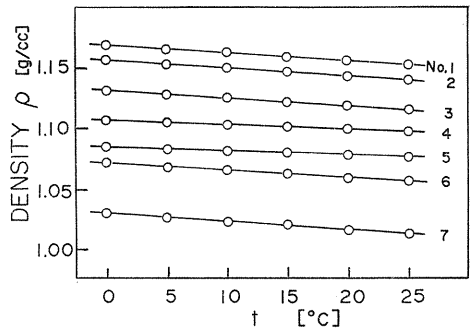

Composition	No. of Sample						
	1	2	3	4	5	6	7
T-NH_3	5.30	6.69	8.68	10.01	11.80	12.29	17.38
T-Cu	1.60	1.58	1.52	1.50	1.37	1.23	1.27
Cu^{II}	0.21	0.22	0.21	0.21	0.21	0.19	0.20
Cu^{I}	1.39	1.36	1.31	1.29	1.16	1.04	1.07
N	3.31	3.96	5.24	6.26	8.03	9.31	12.69
T-CO_2	2.80	2.77	2.66	2.63	2.40	2.20	2.22

FIG. 6. Effect of temperature on the density of copper liquor.

air, sampling of the liquid and the measurement of its density were carried out under sealing with liquid paraffin. Experimental results are shown in Fig. 6. The relationship between the density, ρ [g/cm^3], and the temperature, t [°C] is

$$\rho = -At + B \tag{14}$$

The coefficient A in Eq. (14) for each copper liquor depends on the so-called "copper-ammonia ratio", N, as defined in Chap. 2.1, that is

$$\begin{aligned} 6 \geq N &: A \simeq 0.0007 \\ 6 \leq N \leq 9 &: A \simeq 0.0005 \\ N \geq 9 &: A \simeq 0.0007 \end{aligned}$$

While the plots of a constant B in Eq. (14) against N is shown in Fig. 7 with the effective cuprous concentration [Cu^+] as parameter. Then, B is expressed by

$$B = 1.045 - \left(\frac{1}{34.7}\log[Cu^+] + 0.0079\right)(N - 11.85) \tag{15}$$

where the applicable region of Eq. (15) is as follows;

Total [NH_3] = 3.53 ~ 17.38 moles/l, [Cu^+] = 0.68 ~ 1.39 moles/l; [Cu^{++}] = 0.11 ~ 0.22 moles/l, Total [CO_2] = 1.30 ~ 2.80 moles/l, N = 3.31 ~ 12.69

Furthermore, it was found that the relations mentioned above could be applicable to the hydrochloric or formic copper liquor as well as carbonate liquor used in the experiments. From this coincidence for various copper liquor, usefulness of the copper to ammonia ratio "N" proposed by Onda *et al.*[2] was confirmed.

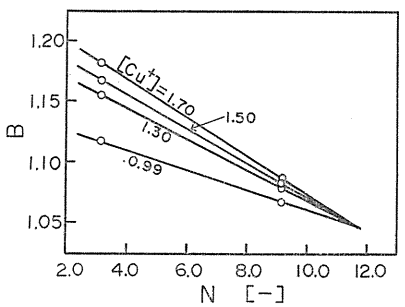

FIG. 7. Relationship between the constant B in Eq. (15) and the copper to ammonia ratio N.

Viscosity of copper liquors

For the same copper liquors as those in the density measurement, viscosities were measured by means of a Ostwald's viscometer in the nitrogen atmosphere. The variation of viscosity of the sample which was left for three weeks, was little within an error of ±0.3%, so that the viscosity data observed would be reliable.

Fig. 8 is the plots of viscosity versus "copper-ammonia ratio", N, with temperature as parameter and shows a little increase of viscosity with the ammonia concentration. Also, it was found that a contribution to viscosity due to the addition of ammonium carbonate is greater than the case of formate. On the other hand, the relationship between the viscosity and temperature would be expressed by Andrade's equation

$$\mu = A' \exp(B'/T) \tag{16}$$

where the coefficients, A' and B', could be determined from the experimental results, respectively. Fig. 9 shows the plot of log μ against $1/T$ for a sample of No. 1, and suggests the applicability to copper liquor of Eq. (16). Then, the comparison between the calculated and observed values is in good agreement.

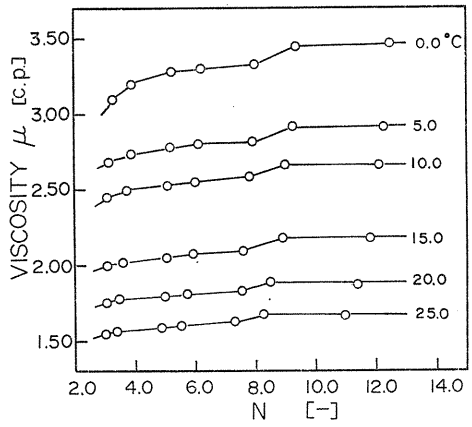

FIG. 8. Effect of the copper to ammonia ratio N on the viscosity of copper liquor.

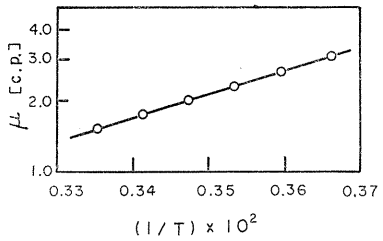

FIG. 9. Relationship between the viscosity of copper liquors and temperature.

When only "copper-ammonia ratio" was varied, the values of A' and B' showed a definite value, respectively, for the region from 4 to 8 of N, then Eq. (16) is expressed by

$$\mu = 5.0 \times 10^{-4} \exp(2400/T) \tag{17}$$

The fact that the values of A' and B' change remarkably at $N \simeq 4$ is consistent with the mechanism reported by Onda *et al.*[2], in which the structure of copper liquor changes at the same value of N.

3.2. Diffusivities in liquid phase

3.2.1. Measurement of the diffusivity by a laminar liquid jet

Knowledge of the diffusivities of dissolved gases in liquids is important in calculating and correlating the gas-liquid mass transfer rate such as gas absorption and distillation. Experimental determination of diffusivity in liquids is inherently difficult because the diffusion process is very slow in liquid phase. Especially, the conventional method by a diaphragm cell (porous disk) has a shortcoming for sparingly soluble gases, because of a difficulty in measuring the small concentration change in solution or a long measuring time over one hundred hours.

On the contrary, the gas absorption rate by the liquid jet can be used to determine the diffusivity and its merits are as follows: jets are simple in design, can be free from ripples, have small end effects, are stable, and have short contact time. Furthermore, the absorption data may be analyzed using the penetration theory provided that the gas molecules penetrate only a short distance into the jet in comparison with its radius, and the velocity across the jet is uniform.

Onda *et al.*[11] had eye to such merits of a laminar jet, and have applied to measuring of the diffusivity in liquids at first in the world. Based on the

penetration theory, the absorption quantity per unit time, N, is expressed by

$$N = 2\pi d(C^* - C_0)\sqrt{D_L v_s l/\pi} \tag{18}$$

where d is the jet diameter; C^* and C_0 are the equilibrium and initial concentrations, respectively; D_L is the diffusivity; l is the jet length; v_s is the surface velocity of liquid jet and is the same as its average velocity, $v_s = 4L/\pi d^2$. Thus, Eq. (18) becomes

$$N = 4(C^* - C_0)\sqrt{D_L L l} \tag{19}$$

in which L is the liquid flow rate (cm³/sec). Then, the plots of N vs. $\sqrt{Ll}$ or N vs. $\sqrt{1/t_c}$ should be a straight line (t_c is the contact time), and its slope is equivalent to $4(C^* - C_0)\sqrt{D_L}$, so that the diffusivity is simply and accurately determined by measuring the absorption rate under conditions of various liquid flow rate or jet length.

The diffusivities of CO_2 in glycerol and cane sugar solutions

The diffusivities of CO_2 in glycerol at 25°C and in aqueous cane sugar solution at 20°C are plotted in Fig. 10 with the values calculated from the Othmer-Thakar's equation[12], in which their coincidence is satisfactory. Also, on the relationship between the liquid viscosity and the diffusivity, it was found that D_L is approximately inversely proportional to μ.

To examine the temperature-dependence of diffusivity, D_L of CO_2 in 25 wt% cane sugar solutions were measured at 5~25°C. Experimental results showed the same temperature-dependence as one in water, that is

$$D_{L,t} = D_{L,20}(1 + 0.03t)/1.6 \tag{20}$$

where $D_{L,t}$ is D_L at t°C: $D_{L,20}$ is D_L at 20°C.

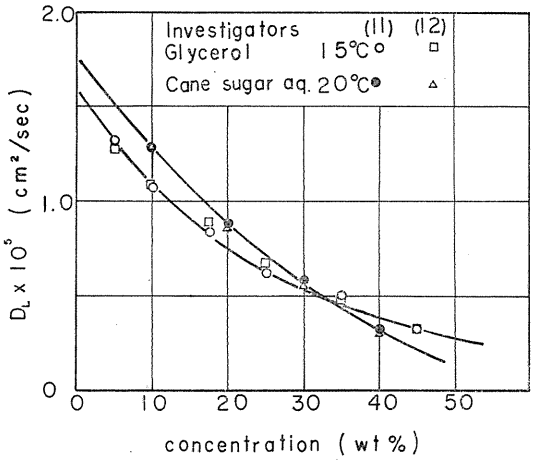

FIG. 10. Diffusivity of CO_2 in glycerine and cane sugar aqueous solutions.

The diffusivity of CO_2 in ethylalchol[11]

In Table 3 and Fig. 11, diffusivities of CO_2 in 99% ethylalchol at various temperature from 6.4 to 20°C are shown. The temperature-dependence of D_L is expressed by

$$D_{L,t} = D_{L,20}\,(1 + 0.35\,t)/1.7 \qquad (21)$$

where t is °C. From Table 3, it is found that $D_L\mu/T$ is constant and its value is 1.40×10^{-7} [cm²•c.p./sec•°K] at any temperature.

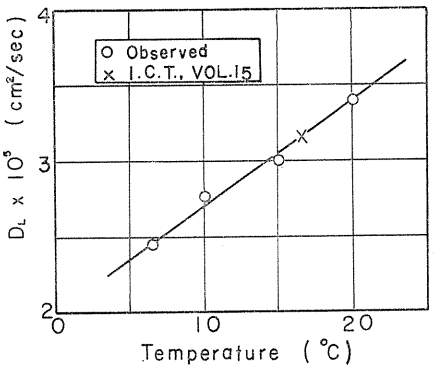

FIG. 11. Diffusivity of CO_2 in 99% ethanol.

TABLE 3. Diffusivities of CO_2 in 99% ethanol at different temperatures

Temp. [°C]	$D_L \times 10^5$ [cm²/sec]	μ [c.p.]	$D_L\mu/T \times 10^7$ [cm²•c.p./sec•°K]
6.4	2.45	1.57	1.38
10	2.78	1.47	1.44
15	3.02	1.33	1.38
20	3.40	1.20	1.39
			mean 1.40

3.2.2. The diffusivities of gases in aqueous electrolyte solutions

The concentration of dissolved gas in liquid is very low under normal conditions, and the viscosity of the solution is essentially the same as that of pure solvent. Under these circumstances, the diffusivity does not vary significantly with concentration and can be predicted with reasonable accuracy by the semi-empirical correlations, for example, Wilke-Chang equation[13]. On the contrary, it is desirable for practical and/or theoretical purposes to make clear the effect of electrolyte on the diffusivity of gases.

For the viscosity of solutions at lower concentrations of electrolyte, Jones-Dole proposed the following equation[19]

$$\mu = \mu_0\,(1 + A\sqrt{C} + BC) \qquad (22)$$

where the term $A\sqrt{C}$ is usually important only at very low concentrations, since $|A|$ is usually much less than $|B|$. The constant B is highly specific and is an approximately additive property of the separate ions. Thus, for relative small solute molecules diffusing in electrolyte solution below about 1 molar, Onda *et al.*[14] assumed the following equation.

$$D/D_0 = 1 - kBC \qquad (23)$$

where D_0 is the diffusivity in pure water: k is a constant value. Based on the experimental results of the diffusivity of CO_2 in water and in aqueous solution of six kinds of salts at 25°C by a laminar jet, the relationship between $d(D/D_0)/$

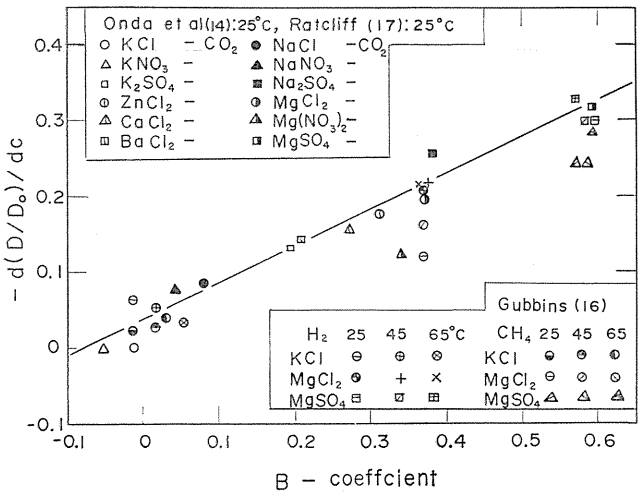

FIG. 12. Relation of $-d(D/D_0)/dC$ and B for the diffusivities of CO_2, H_2 and CH_4 in aqueous electrolyte solutions.

dC and B are plotted in Fig. 12, and then an equation of a best straight line is

$$-\frac{d(D/D_0)}{dC} = 0.036 + 0.485\,B \tag{24}$$

However, for the solution of such salts as KCl and KNO_3 whose viscosity becomes smaller as its concentrations becomes larger within certain ranges of the concentration and temperature, respectively, or are sometimes called to exhibit a "negative viscosity", B-coefficient changes the sign from negative to positive at a point of the minimum viscosity for a salt concentration. For such a salt solution, Jones proposed[19]

$$\mu = \mu_0\,(1 + A\sqrt{C} + B_1C + B_2C^2) \tag{25}$$

where at the concentrations with which we are concerned the term $A\sqrt{C}$ is negligible.

Thus, as a correlation of the diffusivity in salt solution, Onda *et al.*[15] assumed the following equation;

$$D_0/D = 1 + k_1B_1C + k_2B_2C^2 \tag{26}$$

where k_1 and k_2 are the constant to be independent of temperature, a kind of ionic species and the concentration of salt: B_1 and B_2 are determined from the viscosity data as shown in Table 4.

The constants k_1 and k_2 were determined by means of the least square method on the basis of the experimental results and literature values, that is,

$$k_1 = \begin{vmatrix} S_2, & S_1 \\ S_3, & S_4 \end{vmatrix} \Big/ \begin{vmatrix} S_5, & S_2 \\ S_2, & S_3 \end{vmatrix} \qquad k_2 = \begin{vmatrix} S_1, & S_5 \\ S_4, & S_2 \end{vmatrix} \Big/ \begin{vmatrix} S_5, & S_2 \\ S_2, & S_3 \end{vmatrix} \tag{27}$$

TABLE 4. Values of B_1 and B_2 in Eq. (28)

Salt	Temperature [°C]	B_1	B_2
NH_4I	25	−0.0765	0.0134
NH_4Cl	〃	−0.0129	0.0036
NH_4NO_3*	〃	−0.0275	0.0054
KNO_3	〃	−0.0477	0.0254
KCl*	〃	−0.0087	0.0044
KI*	〃	−0.0676	0.0129
KBr	〃	−0.0412	0.0108
K_2SO_4	〃	0.1930	0.0430
$MgCl_2$	〃	0.3240	0.1610
$Mg(NO_3)_2$	〃	0.2470	0.1480
$MgSO_4$	〃	0.5670	0.3740
Na_2SO_4	〃	0.3880	0.1590
$NaNO_3$	〃	0.0634	0.0205
NaCl	〃	0.0867	0.0145
$CaCl_2$	〃	0.2860	0.0620
$BaCl_2$	〃	0.2230	0.0670
$ZnCl_2$	〃	0.3980	−0.0480
NH_4I*	15	−0.0933	0.0137
KNO_3*	〃	−0.0794	0.0323
KI*	〃	−0.1055	0.0174
KI*	5	−0.1527	0.0246

* this work (15)

where

$$S_1 = \sum B_{1i} C_{ij} [1 - (D_0/D)_{ij}]$$
$$S_2 = \sum B_{1i} B_{2i} C_{jj}^3$$
$$S_3 = \sum B_{2i}^2 C_{ij}^4, \qquad S_4 = \sum B_{2i} C_{jj}^2 [1 - (D_0/D)_{ij}]$$
$$S_5 = \sum B_{1i}^2 C_{ij}^2$$

Cosequently

$$D_0/D = 1 + 0.0669\, B_1 C + 0.412\, B_2 C^2 \tag{28}$$

Eq. (28) is applicable to aqueous solution with the concentration below 4 molar of the salt which exert a structure-breaking effect on water.

3.2.3. Measurement of diffusivity by diaphragm cell

In determing the diffusivity of dissolved gas from the absorption rate in liquid jet, the gas solubility in solvent must be known beforehand. While using a diaphragm cell, the diffusivity can be determined by measuring the changes in concentration on each side of the membrane or disk as follows

$$\ln \frac{C_{A1} - C_{A2}}{C_{A10} - C_{A20}} = -D\psi t \tag{29}$$

where ψ is the cell constant and a function of viscosity as well as concentration: C_A with suffix 0 is the intial concentration in the cell 1 or 2.

As the conventional diaphragm is a porous sintered glass or metal disk sealed in a cell, it is necessary for a few days to measure the diffusivity, because the diffusion rate through such disk is very slow and the concentration changes in solution is small. On the contrary, such a shortcoming of diaphragm cell is improved by using a sheet of Millipore filter, so that the measuring time can be shorten to about one hour.

In our laboratary, the diffusivities of CO_2 and H_2S in aqueous salt solution were measured, using a diaphragm cell consisted of two compartments divided with a millipore filter (cellulose-ester type: pore size$=1.2\ \mu$, thickness$=150\ \mu$)[13]. The cell constant was determined to be $5.3\pm0.16\ cm^{-2}$ from the mass transfer rate of KCl through the membrane filter.

To make sure of the reliability of the diffusivity data obtained by the diaphragm cell, those of CO_2 and H_2S in water were measured at 25°C, and were compared with those by liquid jets. For H_2S, there is a little difference between the values reported in literatures, but for CO_2 a good agreement exists. The diffusivities of CO_2 and H_2S in salt solutions are shown in Fig. 13-a and b, and it was found that the agreement between the experimental results and the values estimated by Eq. (28) is within an error of $\pm5\%$.

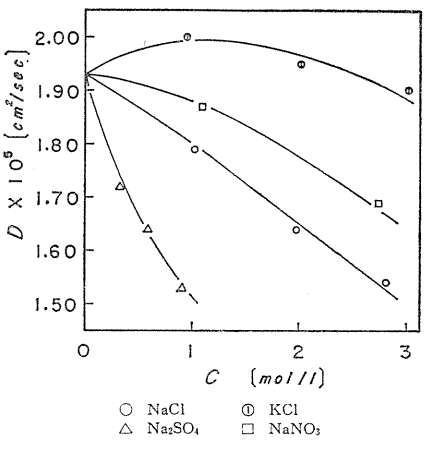

FIG. 13-a. Diffusivity of carbon dioxide in aqueous electrolyte solutions at 25°C.

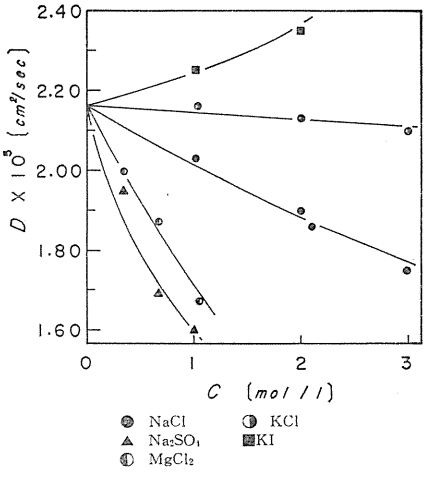

FIG. 13-b. Diffusivities of hydrogen sulphide in aqueous electrolyte solutions at 25°C.

4. Kinetic Studies in Gas-Liquid System

4.1. Absorption of CO_2 into caustic solutions

Concerning with the unsteady absorption of carbon dioxide in alkaline solutions, the following reaction mechanism is considered.

$$CO_2 + H_2O \rightleftarrows H_2CO_3 \qquad (30)$$

$$H_2CO_3 + OH^- \rightleftarrows HCO_3^- + H_2O \quad \text{(instantaneous)} \tag{31}$$

The rate law is pseudo first order

$$-\frac{d[CO_2]}{dt} = k_{CO_2}[CO_2] \tag{32}$$

At pH>11, however, a direct reaction with OH^- predominates

$$CO_2 + OH^- \rightleftarrows HCO_3^- \tag{33}$$

$$HCO_3^- + OH^- \rightleftarrows CO_3^{--} + H_2O \quad \text{(instantaneous)} \tag{34}$$

and the rate law becomes as follows

$$-\frac{d[CO_2]}{dt} = k_{OH^-}[OH^-][CO_2] \tag{35}$$

Reaction (30) which is direct hydration can occur at pH<8, but it has a completely negligible effect at high pH. At pH>11, Reactions (33) and (34) are essentially irreversible since the equilibrium favors the carbonate ion over the bicarbonate ion. Therefore, the only reaction that significantly affect the reaction rate of carbon dioxide with caustic solutions at high $[OH^-]$ concentration, are (33) and (34).

When $[OH^-]>0.5$ moles/l, Onda *et al.*[20] have handled with a pseudo first order reaction, under the assumption that the concentration of hydroxyl ion is uniform in the liquid film because the solubility of CO_2 is small enough compared with hydroxyl ion. Then, the rate equation describing the absorption of CO_2 into a laminar liquid jet may be written by

$$v_s\frac{\partial C}{\partial z} = D_L\frac{\partial^2 C}{\partial x^2} - k'C \tag{36}$$

where v_s, z, x and k' are the surface velocity, the axial direction, the coordinate perpendicular to surface of jet and pseudo first order reaction rate constant, respectively. Boundary conditions are as follows;

$$\left.\begin{aligned} z=0 &: C=0 \\ x=0 &: C=C^* \\ x\to\infty &: C=0 \end{aligned}\right\} \tag{37}$$

The solution of Eq. (36) and the average absorption rate ϕm are as follows;

$$C = \frac{1}{2}C^*\left\{\exp\left(-\sqrt{\frac{k'}{D_L}}x\right)\operatorname{erfc}\left(\frac{x}{2\sqrt{D_Lz/v_s}} - \sqrt{\frac{k'z}{v_s}}\right) + \exp\left(\sqrt{\frac{k'}{D_L}}x\right)\operatorname{erfc}\left(\frac{x}{2\sqrt{D_Lz/v_s}} + \sqrt{\frac{k'z}{v_s}}\right)\right\} \tag{38}$$

$$\phi_m = \sqrt{\frac{D_Lv_s}{\pi z}}C^*\left\{\exp\left(-\frac{k'z}{v_s}\right) + \left(\sqrt{\frac{\pi k'z}{v_s}} + \frac{1}{2}\sqrt{\frac{\pi v_s}{k'z}}\right)\operatorname{erf}\sqrt{\frac{k'z}{v_s}}\right\} \tag{39}$$

When $k'>10^3$ (sec^{-1}), the total amount of CO_2 absorbed, N_A, can be approximated as follows;

$$N_A = 2\pi rl\phi_m \simeq 2\pi rlC^* \sqrt{k' D_L} \tag{40}$$

For the absorption of CO_2 by caustic solutions of LiOH, NaOH and KOH, D_L was estimated from the following relation modified an equation of Stokes-Einstein.

$$D_L \mu^n = \text{constant} \tag{41}$$

where for uni-valency electrolyte solution, n was found to be 0.90 with small variation of the viscosity. On the other hand, gas solubility C^* was predicted by the van Krevelen's method[9].

The rate constants, k_r, of a second order reaction (33) for LiOH, NaOH and KOH are shown in Fig. 14-a, b, and c as the plots of log k_r vs. alkaline concentration. According to Moelwyn-Hughes[28], for dilute solutions the relationship between k_r and ionic strength I is as follows;

$$\log (k_r/k_{ro}) = qI \tag{42}$$

where q is a constant depending on the system: k_{ro} is k_r at infinite dilution.

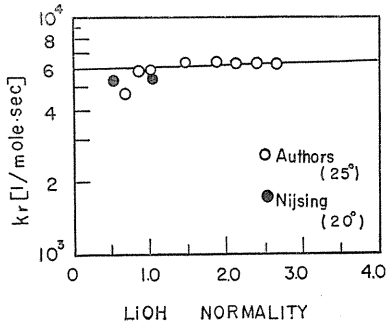

(a) system of LiOH-CO_2

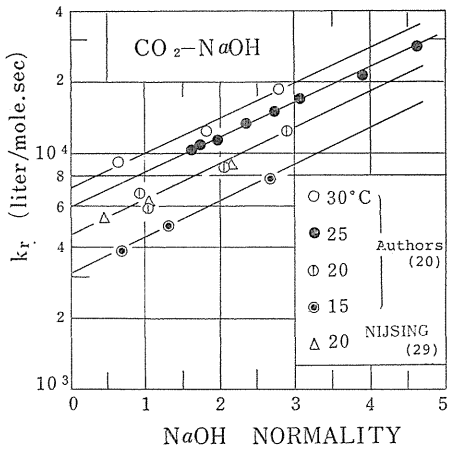

(b) system of NaOH-CO_2

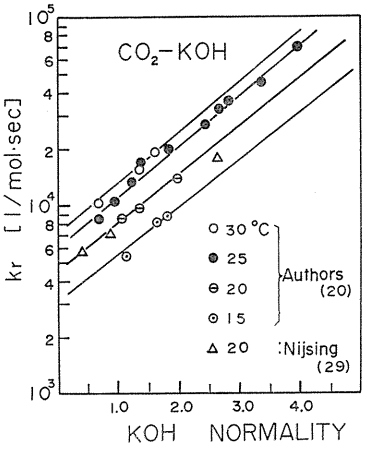

(c) system of KOH-CO_2

FIG. 14. Effect of alkaline concentration on second order reaction rate constant.

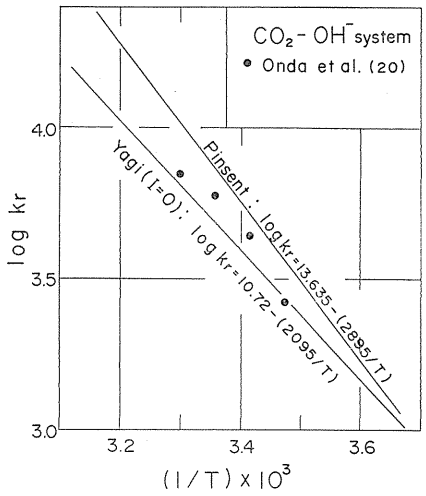

FIG. 15. Arrhenius plots of the reaction rate constant between CO_2 and hydroxyl ion.

By extrapolating to zero concentration in Fig. 14, k_{ro} was found at a given temperature, and the resultant log k_{ro} are plotted against $1/T$ in Fig. 15 as Arrhenius plot together with the literature values. Onda's results[20] are not much different from those obtained with another experimental methods by a few investigators.

4.2. Absorption rate of CO_2 into sodium carbonate solutions containing amino acid or arsenious acid[21]

For the removal of carbon dioxide from gas for industrial use, sodium carbonate or pottasium carbonate is usually used as absorbent. Recently to increase the absorption rate, various substances have been added to carbonate solutions. For instance, sellenious acid, telluic acid, arsenious acid, amino acids etc. are added to the carbonate solution. In general, it is seen that when two or more substances react with carbon dioxide, the absorption rate increased.

The absorption rate of CO_2 into aqueous solutions were measured at 25°C by a laminar liquid jet. From the experimental results for 0.1, 0.3, 0.6 and 1.0 N-Na_2CO_3, it was seen that for a definite contact time the absorption rate of CO_2 decreased with increasing concentration of sodium carbonate. This is because the solubility of CO_2 decreases with increasing Na_2CO_3 as estimated by Eq. (11)

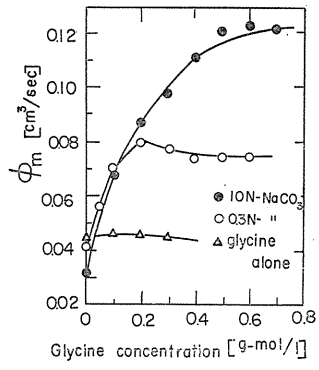

FIG. 16. Rate of absorption of carbon dioxide by sodium carbonate-glycine solutions. $\sqrt{Ll}=3$ (constant).

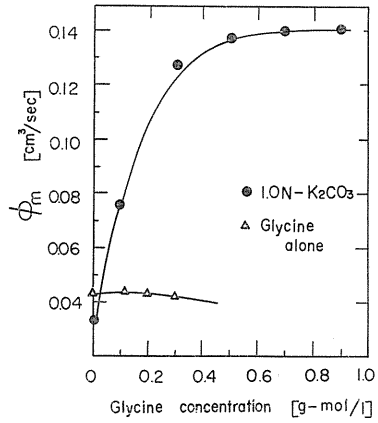

FIG. 17. Rate of absorption of carbon dioxide by 1.0 N potassium carbonate-glycine solutions. $\sqrt{Ll}=3$ (constant).

and the effect of reactions is very small.

In the experimental results for 0.3 and 1.0 N-Na_2CO_3 solutions containing glycine, the absorption rate increases with increasing concentration of glycine, passes through a maximum, and asyptotically approaches a definite value with further increase of added glycine. This behavior is shown in Fig. 16 along with the absorption rate of CO_2 by a solution of glycine. Also, the similar effect of the concentration of sodium glutamate on the absorption rate of CO_2 was found.

Fig. 17 shows the absorption rate of CO_2 by 1.0 N-K_2CO_3 solution to which glycine had been added, along with that by a glycine solution. The results are similar to those obtained when glycine was added to Na_2CO_3 solutions.

For the system of K_2CO_3 and arsenious acid as well as the Vetrocoke process, the effect of arsenious acid on the absorption rate of CO_2 is shown in Fig. 18. Since arsenious acid is almost insoluble in water, the absorption rate of CO_2 in arsenious acid in water could not be determined as was done for amino acids.

The absorption mechanism reasonable for the promotion by these substances mentioned above were also proposed.

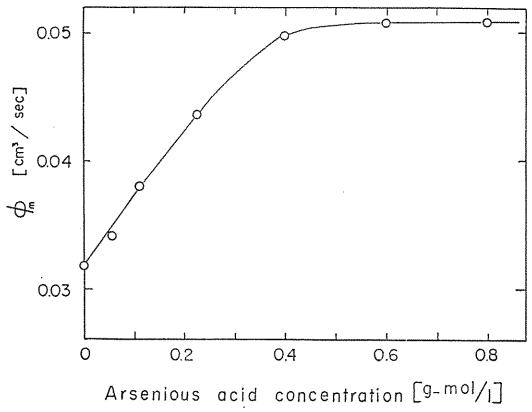

FIG. 18. Rate of absorption of carbon dioxide by 2.0 N potassium carbonate-arsenious acid solutions. $\sqrt{Ll}=3$ (constant)

4.3. Oxidation of sodium sulphite solution

The absorption of oxygen in sodium sulphite solutions in the presence of cobalt sulphate as a catalyst has often been used for the determination of the interfacial area between the gas and liquid in various absorption devices. The reaction of dissolved oxygen with sulphite ion has been studied on the mechanism or reaction rate constants by many investigators, extending over seventy years. However, there are rather poor agreements in their reported data, because the reaction is abnormally long chain reaction, and is sensitive to the catalyst or inhibitor and the concentration of hydrogen ion.

So far, the effect of cobalt sulphate as catalyst on the oxidation rate has been considerably studied, but the quantitative description on pH is not reported. Onda *et al.*[22] have derived the rate equation which depends on the concentrations of cobalt sulphite and hydrogen ion from the data of the oxygen absorption rate irrelevant to sodium sulphite concentration by a wetted wall column.

Assuming that the oxidation rate is proportional to the partial pressure of oxygen gas but is independent of sulphite concentration, from Eq. (40) the absorption rate of oxygen is expressed by

$$N_A = \sqrt{k'D} \cdot C_{Ai} S \qquad (40)'$$

where C_{Ai} is the concentration of gaseous species at the gas-liquid interface; S is the interfacial area.

The plots of N_A vs. l is represented by a straight line, because k', D_A and C_{Ai} in Eq. (40)' are constant, and so the rate constant k' can be determined. Then, the diffusivity of O_2 in sulphite solutions was estimated from the Stokes-Einstein equation. While, the solubility of O_2 in sulphite solutions was evaluated by using the method of van Krevelen similar to Eq. (11). As a result, Eq. (40)' is rewritten by

$$\log (N_A/S) = \log (\sqrt{k'D_A} \cdot C_{Ai}) - 0.351\,[Na_2SO_3] \qquad (43)$$

If the rate constant does not vary with the concentration of sulphite, the plots of $\log (N_A/S)$ vs. $[Na_2SO_3]$ may be located on the straight line as shown in Fig. 19, since a variation of D_A may be small in the range of the concentration concerning in our work. In Fig. 19, the slope of the line fitted to absorption data is -0.377, which deviates 7.4% from the value obtained by solubility data, that is, Eq. (43). On the other hand, the reaction rate constant shows a definite value for the sulphite concentration over 0.23 molar solution as shown in Fig. 20. From Figs. 19 and 20, it is considered that the reaction is first order in oxygen and zero order in sulphite in the range of concentration mentioned above.

For various concentration of cobalt sulphate and hydrogen ion, the reaction rate constants were determined as shown in Fig. 21. The plots of k vs. $[CoSO_4]$ suggests that k is proportional to the concentration of catalyst similar with that of Yagi-Inoue[32]. Fig. 21 shows the plots of $\log k$ vs. pH-value, which shows that $\log k$ is approximated by a linear fuction of pH at a constant sulphite concentration. However, over pH 8.5 as seen from Fig. 21, a corresponding relation

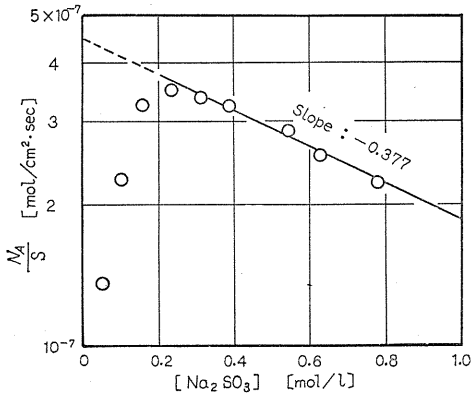

FIG. 19. Absorption rate of O_2 vs. sodium sulphite concentrations(25°C, pH=8.35, $[CoSO_4]$ $=7\times10^{-4}$ mol/l).

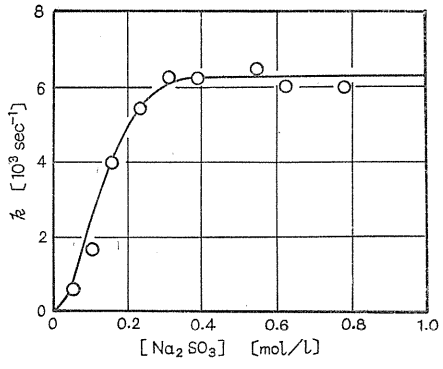

FIG. 20. Reaction rate constant vs. sodium sulphite concentration (25°C, pH= 8.35, $[CoSO_4]=7\times10^{-4}$ mol/l).

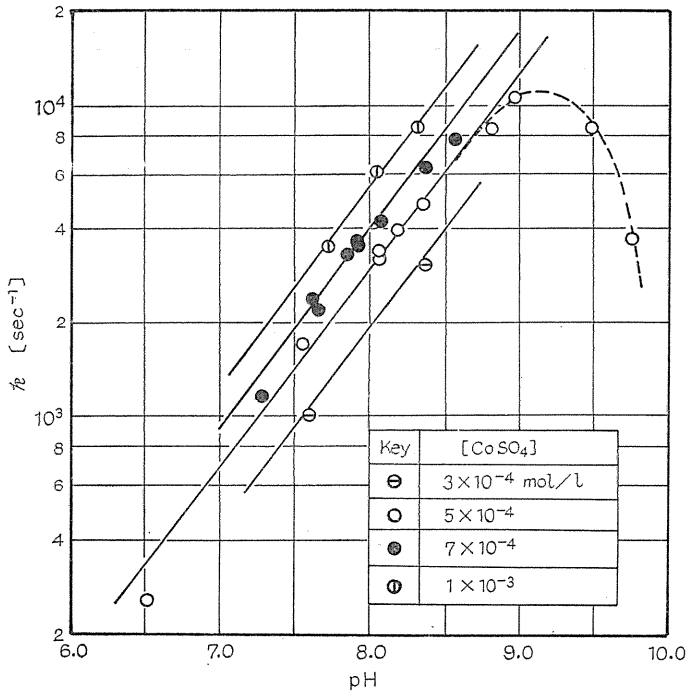

FIG. 21. Reaction rate constant as a function of the pH for various cobaltous sulphate concentrations (25°C, $[Na_2SO_3] = 0.39$ mol/l) Solid lines express Eq. (45).

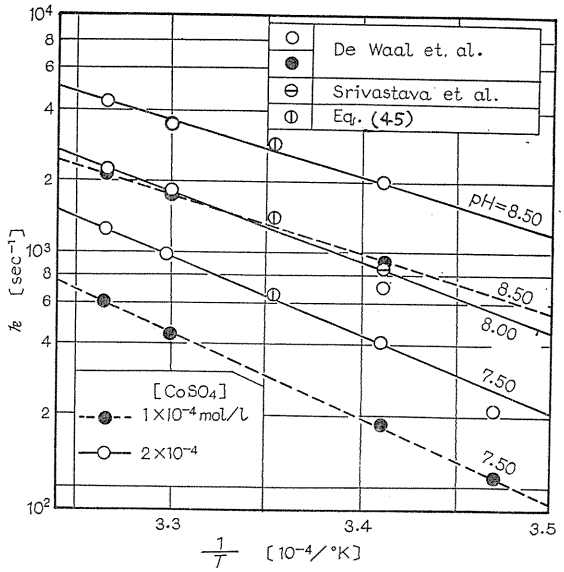

FIG. 22. Reaction rate constant as a function of $1/T$ for various pH.

gradually deviates from the linearity, and at pH 9.2 shows a maximum value.

Fig. 22 shows the Arrhenius plot of k vs. $1/T$ at $[CoSO_4]=1\times10^{-4}$ and 2×10^{-4} moles/l from the literature data. It is found that the activation energy, E, calculated from the slope of the line in Fig. 22 are dependent on pH, but not $[CoSO_4]$. Accordingly, from the plots of E vs. pH, E is correlated with

$$E=(46.5-4.19\ \mathrm{pH})\times10^3 \tag{44}$$

Thus, from Fig. 21 and Eq. (44), the reaction rate constant taken into account the temperature-dependence is expressed by

$$k=3.25\times10^{-3}(1+1.28\times10^4[CoSO_4])[H^+]^{-0.635}\exp\left[\frac{E}{R}\left(\frac{1}{298}-\frac{1}{T}\right)\right] \tag{45}$$

$$288<T<306^\circ\mathrm{K},\ 7.5<\mathrm{pH}<8.5,\ 3\times10^{-4}<[CoSO_4]<10^{-3}\ \mathrm{mol/l}$$

Furthermore, the reasonable reaction mechanism of sulphite oxidation was also proposed and discussed.

4.4. Gas absorption accompanied by complex chemical reaction[23)-26)]

In the years since Hatta[34)] first used the film theory to analyze gas absorption accompanied by an infinitely rapid, irreversible bimolecular reaction, a number of chemical reactions have been treated from the standpoints of the film theory and the penetration theory. These theoretical studies have contributed greatly to the understanding of the effect of a simultaneous chemical reaction on the rate of mass transfer. However, most of the theoretical studies of simultaneous mass transfer and chemical reaction have been developed for such simplified cases, as an irreversible first order reaction or an infinitely rapid reaction. In the commercially important chemical reactions, however, there are many cases where the mechanisms of the simultaneous chemical reactions are complex, such as reversible, consecutive and parallel reactions, and the reaction rates are represented by complex functions of the concentrations of the dissolved gas and the reactants in the liquid phase.

Onda *et al.* have given the approximate solutions based on the film theory for gas absorption accompanied by the following complex chemical reaction.

a)[23)] $(m, n)-(p, q)$-th order reversible reaction with four chemical species which is m-th order with respect to a solute A, n-th order with respect to a reactant in liquid, B, and p-th and q-th order with respect to products E and F, respectively,

$$aA(g)+bB(l)\rightleftarrows eE(l)+fF(l) \tag{46}$$

b)[24)] $(m, n)-(p, q)$-th order consecutive reaction

$$\left.\begin{aligned}&aA(g)+bB(l)\rightarrow cC(l)+\mathrm{product}\\&a'A'(g)+cC(l)\rightarrow bB(l)\end{aligned}\right\} \tag{47}$$

$$\left.\begin{aligned}&aA(g)+bB(l)\rightarrow cC(l)\\&aA(g)+c'C(l)\rightarrow\mathrm{product}\end{aligned}\right\} \tag{47}'$$

c)[25)] $(m, n)-(p, q)$-th order parallel reaction

$$\left.\begin{array}{l} aA(g)+bB(l)\rightarrow \text{product} \\ aA(g)+cC(l)\rightarrow \text{product} \end{array}\right\} \quad \cdots\cdots\cdots\cdots \quad (48)$$

$$\left.\begin{array}{l} aA(g)+bB(l)\rightarrow \text{product} \\ a'A'(g)+bB(l)\rightarrow \text{product} \end{array}\right\} \quad (48)'$$

These approximate solutions were compared with analytical or numerical solutions to check the accuracy of the approximation in the graphical form. The difference between the approximate and exact solutions are only a few per cent for all cases.

In addition for gas absorption accompanied by $(m, n)-(p, q)$-th order reaction mentioned above, the approximate solutions based on the penetration and surface renewal theories were derived under the condition of equal diffusivities, and compared with the approximate solution based on the film theory to manifest the generalized solution being suitable for three theories. For the case of reversible reaction, the approximate solution based on the penetration theory was compared with the numerical solution to examine the accuracy of Hikita-Asai's approximation[35] in the unsteady state. It was found that the deviation of the approximate solution from the numerical solution is only a few per cent[26].

4.5. Gas absorption with chemical reaction under the cosideration of ionic strength[36]

Numerous investigations on gas absorption are mostly on the performance of various gas-liquid contactors and/or the absorption mechanism or the prediction of reaction factor. However, it is also important to investigate the effect of a kind of absorbent on the gas absorption rate. On the absorption of CO_2, it has been made clear that the absorption rate does not always increase with the concentration of alkali, and increased by adding an amine to sodium or potassium carbonate solution as mentioned in Chap. 4.2.

In general, the gas absorption rate depends on physicochemical properties in the vicinity of gas-liquid interface, *i.e.* the gas solubility, diffusivity and reaction rate constant, which are expressed by a function of the ionic strength in liquid phases. Moreover, the equilibrium between ions in liquid phase must be taken into consideration.

The relationship between the absorption rates and ionic strength for three absorption processes were examined theoretically and experimentally by using these functions above mentioned, and the following conclusions are obtained.

1) In physical absorption process, as ionic strength increases, the absorption rate decreases for $K_s>0$, where K_s is the salting-out parameter, but in the case of $K_s<0$, the absorption rate increases.

2) In gas absorption accompanied by a pseudo m-th order chemical reaction, there are some cases for which the relationship between absorption rate and ionic strength becomes convex.

3) In gas absorption accompanied by instantaneous chemical reaction, the absorption rate increases with increasing ionic strength in liquid phase.

4.6. Behavior of the reaction plane movement in gas absorption with instantaneous chemical reaction[37]

For an analysis of gas absorption accompanied by an instantaneous chemical

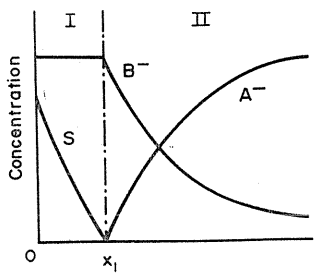

Model (1) : $K_1 \to \infty$, $K_2 = 0$

$S + A^- \to B^-$

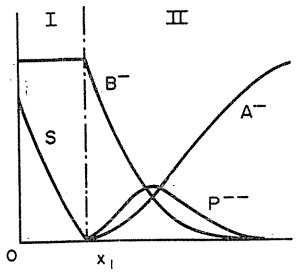

Model (2) : $K_1 \to \infty$, K_2 = finite

$S + A^- \to B^-$

$B^- + A^- \rightleftharpoons P^{--}$

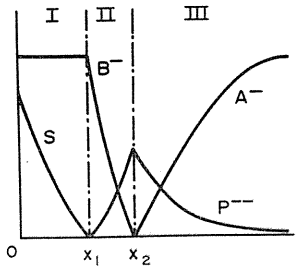

Model (3) : $K_1 \to \infty$, $K_2 \to \infty$, $K_1/K_2 \to \infty$

$S + A^- \to B^-$

$B^- + A^- \to P^{--}$

$S + P^{--} \to 2B^-$

x_1 : the first reaction plane

x_2 : the second reaction plane

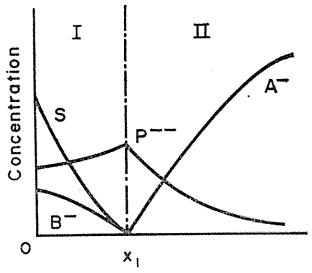

Model (4) : $K_1 \to \infty$, $K_2 \to \infty$

K_1/K_2 = finite

$S + A^- \to B^-$

$B^- + A^- \to P^{--}$

$S + P^{--} \rightleftharpoons 2B^-$

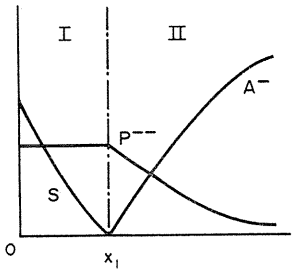

Model (5) : $K_1 \to \infty$, $K_2 \to \infty$, $K_1/K_2 \to 0$

$S + 2A^- \to P^{--}$

FIG. 23. Plausible concentration profiles for reaction (ii) at $K_1 \to \infty$ and various values of K_2. I, II, III: diffusion regions; -----: reaction plane.

reaction based on the penetration theory, an understanding of the reaction plane appears to be essential since it is characterized by interaction between chemical reaction and mass transfer processes.

On the behavior of the reaction plane movement, Onda *et al.* discussed in the model based on the following two-step chemical reaction

$$S + A^- \underset{\leftarrow}{\overset{K_1}{\rightarrow}} B^- \qquad \text{(i)}$$

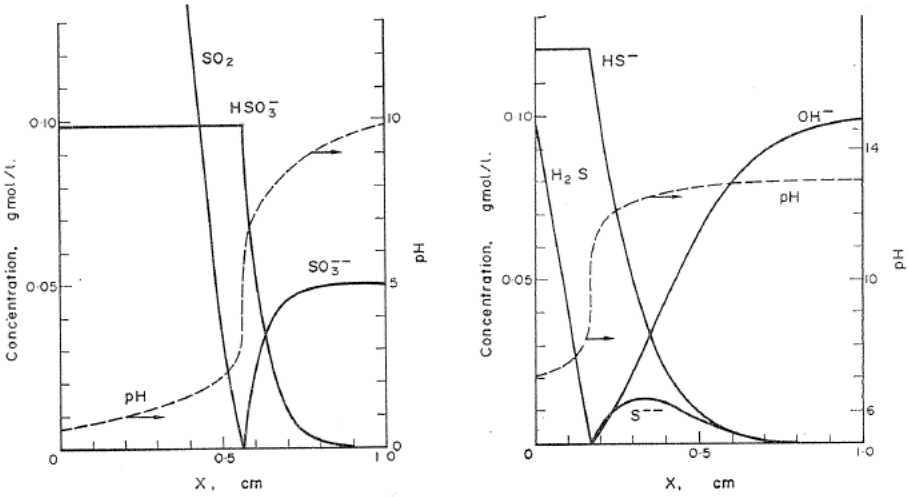

(a) SO_2-0.0500 g-mol/l Na_2SO_3 system (b) H_2S-0.100 g-mol/l NaOH system

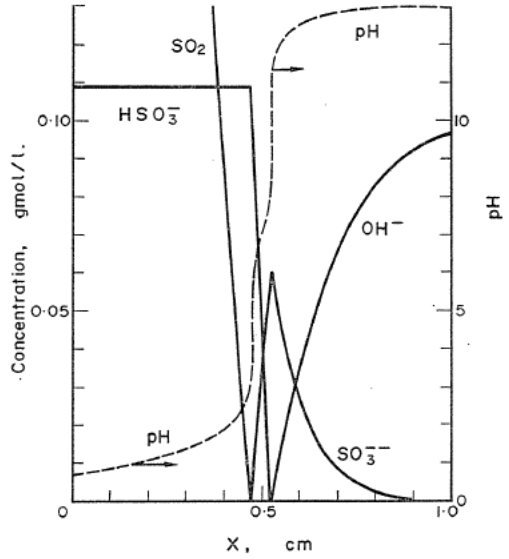

(c) SO_2-0.100 g-mol/l NaOH system

FIG. 24. Concentration profiles calculated by analytical solutions and chemical equilibria at the exposure time $t=30$ min.

$$B^- + A^- \underset{\leftarrow}{\overset{K_2}{\rightleftharpoons}} P^{--} \qquad \text{(ii)}$$

Plausible sketches of the concentration profiles in these models are shown in Fig. 23 for various values of equilibrium constant of reaction (ii), K_2, at $K_1 \to \infty$.

The absorption of sulphur dioxide and hydrogen sulphide into jelly containing sodium sulphite or sodium hydroxide aqueous solution were investigated by measuring the movement of reaction plane denoted by change of the color tone of indicator. The experimental results were compared with the analytical solutions based on the penetration theory.

In Fig. 24, the concentration profiles calculated from the solutions of Models (1), (2) and (3) for SO_2-Na_2SO_3, H_2S-NaOH and SO_2-NaOH reaction systems, respectively, are shown at the exposure time $t=30$ min. The profiles of pH evaluated by the chemical equilibria of reaction systems are shown simultaneous by the broken line, because the chemical equilibria may be assumed to hold at any point in the liquid phase, though each reaction is instantaneous and concentration gradients exist in the liquid. On the other hand, the color of jelly contained in a cylindrical glass tube for each chemical reaction is shown in Fig. 24 A. The distances form an end of a cylindrical glass tube to the color-change planes, x_1 and x_2, were measured by a microscope.

The reaction between sulphur dioxide and sodium sulphite was found to be expressed by Model (1) as shown in Fig. 25 plotted as βa vs. $C_{Na_2SO_3}$. The absorption process of hydrogen sulphide into sodium hydroxide solution was confirmed to be refered to Model (2) whose solution can't be obtained analytically except for the case of equal diffusivity, $D_S = D_A = D_P$. The reaction between sulphur dioxide and sodium hydroxide was verified to be a two-step consecutive instantaneous chemical reaction by substantiating the presence of the second

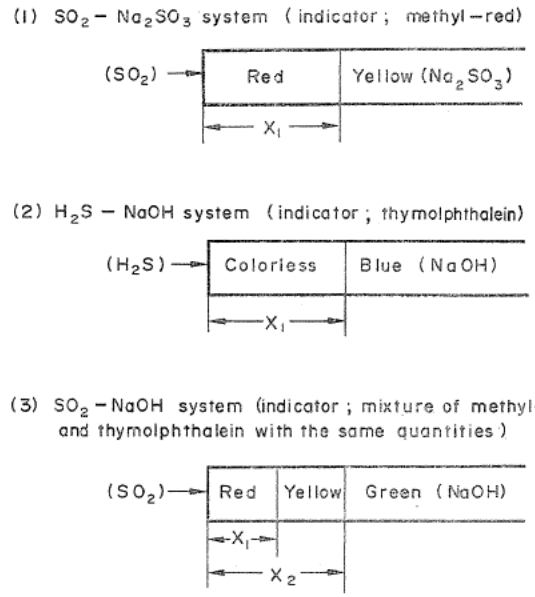

FIG. 24 A. Color-tones of jelly contained in cylindrical glass tube.

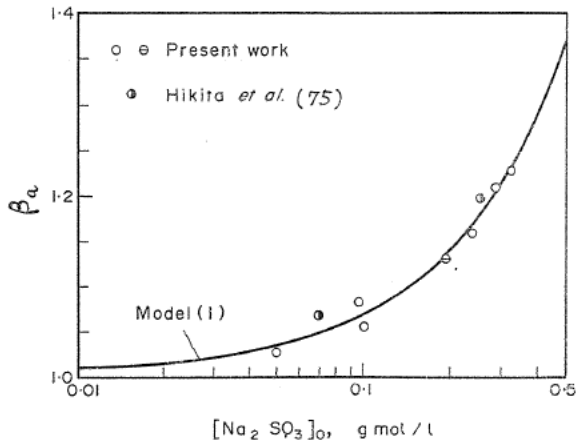

FIG. 25. β_a vs. $[Na_2SO_3]_0$ for SO_2-Na_2SO_3 system.

reaction plane, and the experimental results are in good agreement with the theoretical solution of Model (3).

5. Effective Surface Area in Packed Columns

Mass transfer coefficients for gas absorption, desorption and vaporization in packed columns have been studied by many investigators. Separation of capacity coefficients k_Ga and k_La, into their constituents, the mass transfer coefficients, k_G or k_L, and the specific interfacial area, a, was attempted by Weisman-Bonilla[48] and Shulman *et al.*[49]. Dependence of k_G, k_L and a on the physico-chemical properties of gas and liquid system and the operating variables are essentially different.

There are two methods for estimating the effective surface area, that is

1) Using the apparatus whose surface area is known and assuming the flow patterns of liquid and gas are the same as those in packed columns, the mass transfer coefficients were estimated.

2) The wetted surface area of packings, a_w, can be measured, and then, $k_G=k_Ga/a_w$ or $k_L=k_La/a_w$.

In the former case, it was concluded by Hikita[50] that a from k_Ga is different to a from k_La. On the contrary, the second method is easily carried out, and under the assumption that the wetted surface area equal to the effective surface area, a, the correlation for a_w can be presented.

A few equation to obtain the wetted surface area on irrigated packings have been proposed. Hikita-Kataoka[47] reported an equation of a_w for Raschig rings, which contains the liquid surface tension. However, these correlations did not take into account the surface effect of packing material on the wetted surface area.

Effects of variables on a_w

The packing pieces and the properties of irrigating liquids used for measurement of wetted area[42)43)45)] are shown in Table 5 with those in the literatures.

TABLE 5. Properties of liquid used for measurement of wetted surface area

Size	Material	Liquids	ρ [kg/m³]	μ [kg/m-hr]	$\sigma\times10^{-5}$ [kg/hr²]	Keys of Fig.	Ref.
Packing piece: Sphere ($a_tD_P=3.4$)							
0.5″	ceramic	water	998	3.62	8.63	0.5 S-W	(43)
	〃	water*	998	3.62	6.43	0.5 S-WS	〃
	〃	ethanol	970	6.97	5.28	0.5 S-WE	〃
1″	〃	cane sugar	1147	13.5	8.70	1.0 S-WC	〃
	〃	water	998	3.62	7.30	1.0 S-W	〃
	glass	water	998	3.01	7.30	1.0 SG-W	(45)
Berl saddles ($a_tD_P=5.6$)							
0.5″	ceramic	water	998	3.6	8.70	0.5 B-W	(45)
1.0″	〃	water	998	2.9～3.3	8.3～8.4	1.0 B-W	〃
	〃	water*	998	3.29	6.39	1.0 B-WS	〃
1.5″	〃	water	998	2.9～3.4	8.2～8.7	1.5 B-W	〃
	〃	water*	998	3.65	5.7～6.4	1.5 B-WS	〃
2.0″	〃	water	998	3.72	9.45	2.0 B-W	〃
Raschig rings ($a_tD_P=4.7$)							
8 mm	ceramic	water	998	4.00	8.70	8 R-W	(45)
	〃	water*	998	3.62	5.23	8 R-WS 1	〃
	〃	water	998	3.62	6.87	8 R-WS 2	〃
	〃	ethanol	970	7.30	5.17	8 R-WE	〃
	〃	glycerol	1072	9.00	8.65	8 R-WG 1	〃
	〃	glycerol	1156	39.0	8.65	8 R-WG 2	〃
	〃	cane sugar	1147	13.5	8.73	8 R-WC	〃
15 mm	ceramic	water	1000	5.04	7.80	15 R-W 1	(55)
	paper	water*	996	2.88	4.37	15 R-WS	(47)
	〃	water	996	2.88	8.39	15 R-W 2	〃
25 mm	ceramic	water	1000	5.06	7.80	25 R-W 1	(55)
	paper	water	996	2.88	8.39	25 R-W 2	(47)
	〃	water*	997	3.20	3.86	25 R-WS 1	〃
	〃	water*	997	3.20	4.96	25 R-WS 2	〃
	〃	water*	997	3.20	6.56	25 R-WS 3	〃
	〃	water	997	3.20	8.48	25 R-W 3	〃
	paper	glycerol	1140	13.8	7.69	25 R-WG 1	〃
	〃	glycerol	1080	6.05	8.00	25 R-WG 2	〃
	〃	methanol	948	4.86	5.18	25 R-WM	〃
35 mm	ceramic	water	1000	5.04	7.80	35 R-W 1	(55)
	paper	water*	996	2.88	4.37	35 R-WS	(47)
	〃	water	996	2.88	8.39	35 R-W 2	〃
	〃	glycerol	1150	13.8	7.75	35 R-WG	〃

* added the surface active agent

The colored liquid in which a Rohdamine was added, were irrigated over the packed beds through a distributor. For glass sphere, however, the aqueous solution of lead nitrate were used, because the colored area on glass could not measured accurately, and $Pb(NO_3)_2$ deposits as PbS on wetted surface of packings by a reaction with H_2S gas. After irrigation of 15 minutes, the static hold-up was vaporized under vaccum conditions, and was dried by a hot air. Then, colored area on each packing piece was measured by means of the specific devices.

The effect of irrigation time on a_w for 10 mm Raschig rings is shown in Fig. 26. The wetted area becomes constant at 6~8 minutes after the start of irrigation and the reproducibility of the a_w-measurement is also satisfactory.

The effect of liquid flow rate for 8 mm Raschig rings are shown in Fig. 27 as an example. Also, it was found that the observed values for Berl saddles and spheres and the literature values for 15, 25 and 35 mm Raschig rings, respectively, show the same dependence on liquid flow rate, which have a slope of 0.4. As a result, the effect of L on a_w is expressed by

$$-\ln(1-a_w/a_t) \propto L^{0.4} \tag{49}$$

The data in Fig. 27 for the liquid surface tension ranging from 8.5×10^5 to

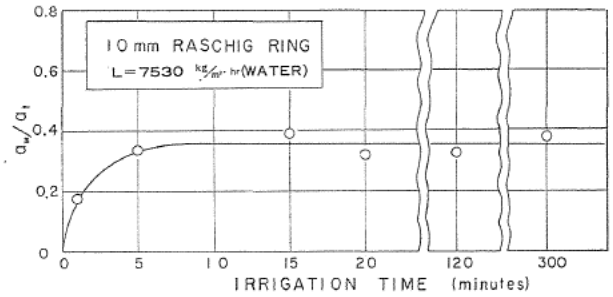

FIG. 26. Relation between irrigation time and wetted area.

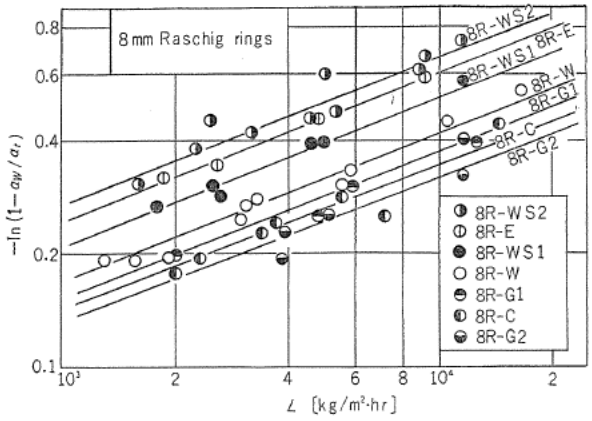

FIG. 27. Experimental results of wetted areas for Raschig rings.

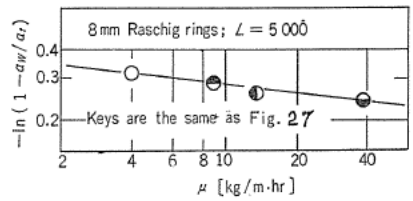

FIG. 28. Effect of viscosity on wetted areas.

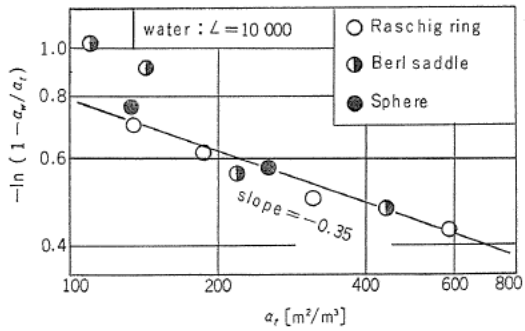

FIG. 29. Effect of total surface area on wetted areas.

8.73×10^5 kg/hr² at L=5,000 kg/m²·hr are plotted in Fig. 28 against the liquid viscosity. A straight line fitted for the data points has the slope of -0.10, that is;

$$-\ln(1-a_w/a_t)\propto\mu^{-0.10} \tag{50}$$

Effects of packing shape and size on a_w may be discussed with a characteristic values of packing, a_t. Values of $-\ln(1-a_w/a_t)$ for three kinds of packings with the solutions of $\sigma=8.5\times10^5$ kg/hr² and $\mu=3.6$ kg/m·hr are plotted against a_t of Raschig rings, Berl saddles and spheres in Fig. 29. A straight line fitted for the points in Fig. 29 has a slope of -0.35, that is:

$$-\ln(1-a_w/a_t)\propto a_t^{-0.35} \tag{51}$$

It is considered that the surface tension of liquid, σ, has a great influence upon the wettability of packing. This effect is found by taking into account the relations of (50) and (51). The values of $-a_t^{0.35}\mu^{-0.1}\ln(1-a_w/a_t)$ calculated at L=5,000 kg/m²·hr are plotted in Fig. 30 against σ and these points are correlated with a straight line having a slope of -0.95, that is;

$$-\ln(1-a_w/a_t)\propto\sigma^{-0.95} \tag{52}$$

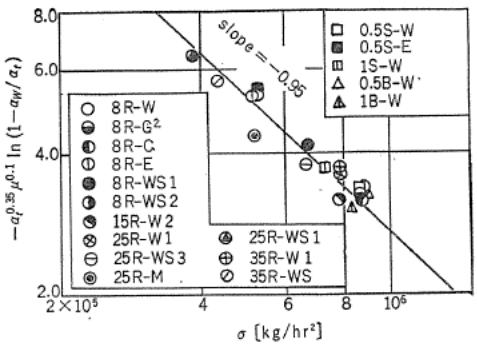

FIG. 30. Effect of surface tension on wetted areas.

Surface effect of packing material

The contact angle formed by a drop on the ceramic plate is not distinct and changes with time because of surface roughness. In our study[45], the level surface method that is called the plate method was employed. This principle is that the quadrilateral plate partly immersed in liquid surface remains level right up to the line of contact with the plate. Then, the angle made by the plate with the horizontal is the contact angle. This observation was carried out with a naked eye or a travelling microscope.

It is necessary to prepare the same surface with one of packing materials. Hence, the following solid plates were used; ① glass, ② common ceramic, ③ mixture of earthen ware and common ceramic, ④ ceramic of fine quality, ⑤ lusterless polyvinyl-chloride (the characteristic of surface is the same as one of tube), ⑥ lusterous polyvinylchloride. The liquids used were the various concentration of potassium carbonate, sodium hydroxide and ethanol aqueous solutions. All measurement were made at 20°C.

Results on the contact angle are plotted in Fig. 31 against the liquid surface tension, in which the literature values for glass, P.V.C., polyethylene and paraffin surface are shown.

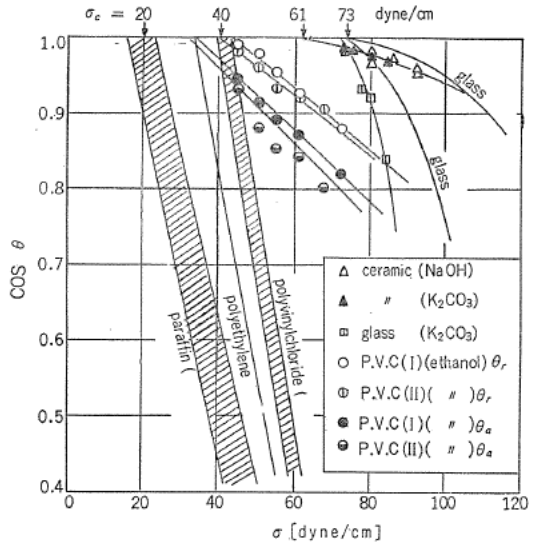

FIG. 31. Experimental results of contact angle at 20°C.

For the relation between $\cos\theta$ and σ, Zisman *et al.*[51] have shown that the increase in $\cos\theta$ with decreasing liquid surface tension is linear for a given solid. He defined a critical surface tension σ_c, when θ just equals 0°, *i.e.* this value of σ_c for a solid is indicative of surface energy, and the liquid spreads for all values of σ below σ_c. In other word, the surface having a high value of σ_c is more wettable. Hence, σ_c was introduced to correlate the wetted surface area on packings as a characteristic property with respect to the wettability.

In Fig. 31, the line through the data points have been extrapolated to the value of $\cos\theta=1$ and σ_c are determined. The values of σ_c for various materials

TABLE 6. Values of critical surface tension at 20°C

glass	73 [dyne/cm]	
ceramic	61 [〃]	
polyvinyl chloride	40 [〃]	
carbon	60~65 [〃]	(estimated)
steel	71 [〃]	
paraffine	20 [〃]	

are shown in Table 6.

On the other hand, to ascertain the surface effect on a_w, that is the effect of σ_c, numerous data on k_La for various packing material are necessary. In our studies[45], the absorption of pure CO_2 into water were carried out with the packing of various shapes and materials. For the indentical shape packing and liquid flow rate, it was assumed that the difference of k_La measured would be merely caused by a_w. Based upon this assumption, the wetted area could be predicted by dividing the value of k_La with k_L calculated from our previous correlation[43].

$$k_L(\rho_L/\mu_L g)^{1/3} = 0.11(L/a_t\mu_L)^{1/2}(\mu_L/\rho_L D_L)^{-1/2}(a_t D_P)^{-1.0} \tag{53}$$

which also was obtained on the basis of wetted area. Now, let's represent a resultant wetted area by a'_w. It is the wetted area calculated from Eq. (53), and by this method the wetted surface area for such material as P.V.C. and paraffin etc. which can not be directly observed were determined.

a'_w thus obtained for 25 mm Raschig rings are plotted against the liquid rate in Fig. 32. Similar relations were obtained for 1″ glass and ceramic spheres and 13 mm ceramic and P.V.C. rods, respectively. As seen in Fig. 32, having the same effect of L on a'_w for ceramic, P.V.C. and praffin, it is suggested that the above mentioned assumption is satisfied. Thus, the values of $-\ln(1-a'_w/a_t)$ at

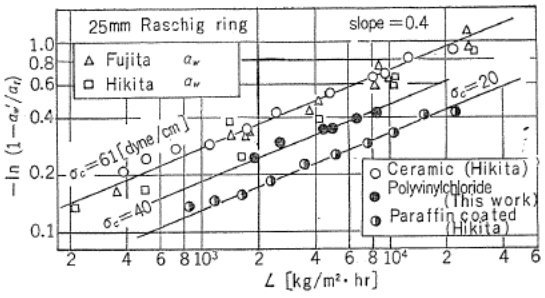

FIG. 32. Comparison of wetted areas by packing material for Raschig ring.

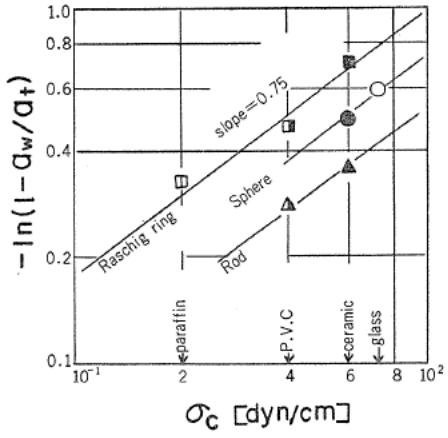

FIG. 33. Effect of critical surface tension on wetted areas.

L=10,000 kg/m²·hr are plotted in Fig. 33 against σ_c of each packing material. The straight lines through the points for three kinds of packings have the same slope of 0.75, respectively, that is;

$$-\ln(1-a_w/a_t) \propto \sigma_c^{0.75} \tag{54}$$

The effects of individual variables on a_w are represented by the relations (49), (50), (51), (52) and (54), that is;

$$-\ln(1-a_w/a_t) \propto L^{0.4}\mu^{-0.1}a_t^{-0.35}\sigma^{-0.95}\sigma_c^{0.75} \tag{55}$$

Taking the gravitational constant, g, and the liquid density, ρ, into consideration, four dimensionless terms of (σ_c/σ), Reynolds, Weber, and Froude number have been obtained. From the relation (55), the powers of these dimensionless terms are determined as follows;

$$\begin{aligned}-\ln(1-a_w/a_t) &= n(L/a_t\mu)^{0.1}(a_tL^2/\rho^2g)^{-0.05}(L^2/\rho\sigma a_t)^{0.2}(\sigma_c/\sigma)^{0.75}\\ &= nRe^{0.1}Fr^{-0.05}We^{0.2}(\sigma_c/\sigma)^{0.75}\end{aligned} \tag{56}$$

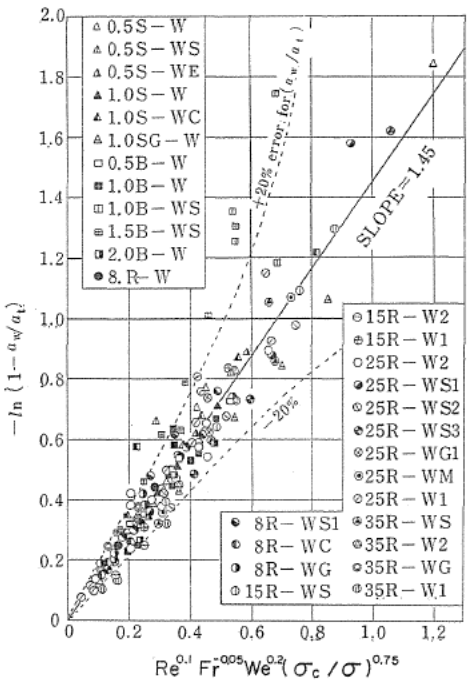

FIG. 34. Correlation of wetted area for various packings.

where a constant, n=1.45, is determined from the slope of a straight line drawn in Fig. 34, which all the data of a_w for the systems shown in Table 5 are plotted with the relation (56). The broken lines in Fig. 34 shows the range of ±20% error as a_w/a_t. Although the data apparently are scatterd, the greater parts of points are within an error of ±10%. Then, a_w can be represented by

$$a_w/a_t = 1-\exp\left\{-1.45\left(\frac{L}{a_t\mu}\right)^{0.1}\times\left(\frac{a_tL^2}{g\rho^2}\right)^{-0.05}\left(\frac{L^2}{\rho\sigma a_t}\right)^{0.2}\left(\frac{\sigma_c}{\sigma}\right)^{0.75}\right\} \tag{57}$$

The applicable region of Eq. (57) is

$0.04<(L/a_t\mu)<500$, $1.20\times10^{-8}<(L^2/\rho\sigma a_t)<0.27$, $2.5\times10^{-9}<(a_tL^2/g\rho^2)<1.8\times10^{-2}$, $0.3<(\sigma_c/\sigma)<2.0$.

6. Mass Transfer Coefficients in Packed Column

To predict the individual phase coefficients, correlations of the gas absorption data are important for reliable design of gas absorption equipment. On liquid

phase mass transfer coefficients in packed columns, Sherwood-Holloway[54] published an empirical correlation of HTU which is recognized as the most reliable at present. While, on the gas phase transfer, there is a considerable discrepancy in the data concerning the effect of various variables.

It is obvious that the mass transfer coefficient, k, and the interfacial area, a, depend on physico-chemical properties of the gas-liquid system and the operating variables in different ways, because k depends on the diffusivity and film thickness, or contact time, but a does not. Accordingly, it is very important to separate the capacity coefficient into k_G or k_L and a, and to correlate them within a reasonable error.

6.1. Liquid phase mass transfer coefficient; k_L

Liquid phase mass transfer coefficients for the gas absorption and deporption in a specially made apparatus having the known interfacial area, for example, a bead column or disk column, had been obtained by several investigators. In these methods, a known interfacial area of the column whose flow pattern is considered to be similar to one on packings had been used to obtain k_L, so that it includes the assumption that k_L in the bead column, disk column and packed column are identical each other for the same liquid rate. But this assumption can not be conceivable.

By the reasons metioned above, Onda *et al.*[38)39)] obtained the k_L by separating from k_La with the wetted surface area, assuming that a_w is identical to the effective surface area. From the standpoints of the two-film and the penetration theories, respectively, the correlations of k_L with Reynolds and Schmidt number were discussed for the packings of Raschig ring, and the coincidence between the equations based on both the theories was most satisfactory by

$$k_L(\rho_L/\mu_L g)^{1/3} = C(L/a_t\mu_L)^{1/2}(\mu_L/\rho_L D_L)^{-1/2} \tag{58}$$

where

$$C = 0.01 \sim 0.02$$

Furthermore, in order to clarify the effect of shape of packings on k_L, a_w for Berl saddles and spheres were measured and correlated, respectively[43]. As a result, k_L obtained for three kinds of packings as mentioned above were also correlated by Eq. (53) within an error of $\pm 20\%$.

However, as the modified equation of a_w has been proposed later, the correlation of k_L, Eq. (53), must be corrected on the basis of Eq. (57). For the k_La data on typical packings, a'_w calculated by Eq. (53) are plotted in Fig. 35 as well as Fig. 34, where it was assumed that Eq. (53) could be applicable to Pall rings and rods, using (a_tD_P) shown in Table 7. As seen in Fig. 35, it is found that the linear relations with various slopes differ from a_w represented by a dotted line, except for Raschig rings. Approximately, the following relation is obtained[45].

$$a'_w/a_w \simeq 0.136\,(a_tD_P)^{1.40} \tag{59}$$

Hence, the correction of Eq. (53) with Eq. (59) can be represented by

$$k_L\left(\frac{\rho_L}{\mu_L g}\right)^{1/3} = 0.015\left(\frac{L}{a_t\mu_L}\right)^{1/2}\left(\frac{\mu_L}{\rho_L D_L}\right)^{-1/2}(a_tD_P)^{0.4} \tag{60}$$

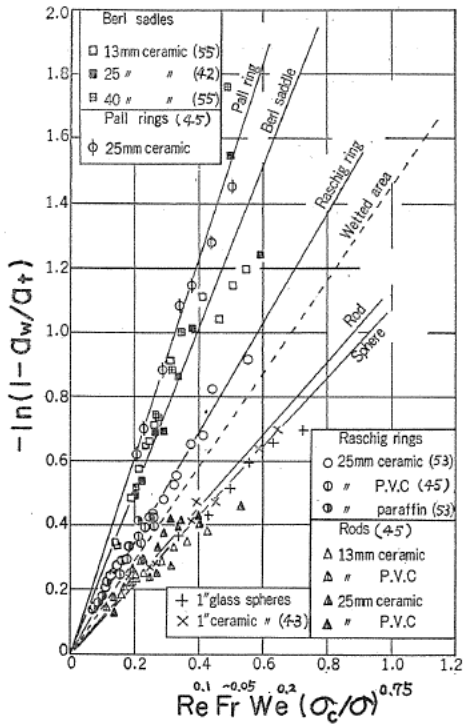

FIG. 35. Wetted area calculated by Eq. (53).

TABLE 7. Values of shape factor: a_tD_P

Rasching rings	4.7
Berl saddles	5.6
Speres	3.4
Rods (same dia. and height)	3.5
Pall rings	5.8
Interlox saddles	7.1

Eq. (60) is shown by a straight line in Fig. 36, which would correlate the k_L obtained from our data and the literatures data for various packings within an error of $\pm 20\%$, but for the greater parts of reliable data the error is within $\pm 10\%$.

However, for water with and without surfacant when the same liquid rate is used, k_La for the surfactant solutions usually are smaller than those for the pure water. On the contrary, for a surfactant solution k_La_w estimated as the product of Eq. (60) by Eq. (57) is contradictory with a experimental fact.

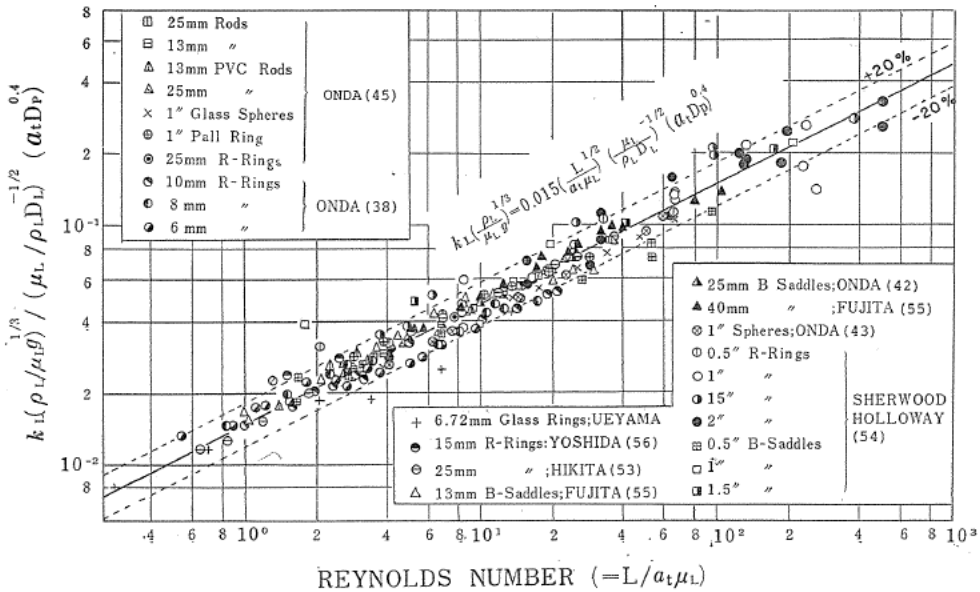

FIG. 36. Dependence of k_L on Re with various packings for water.

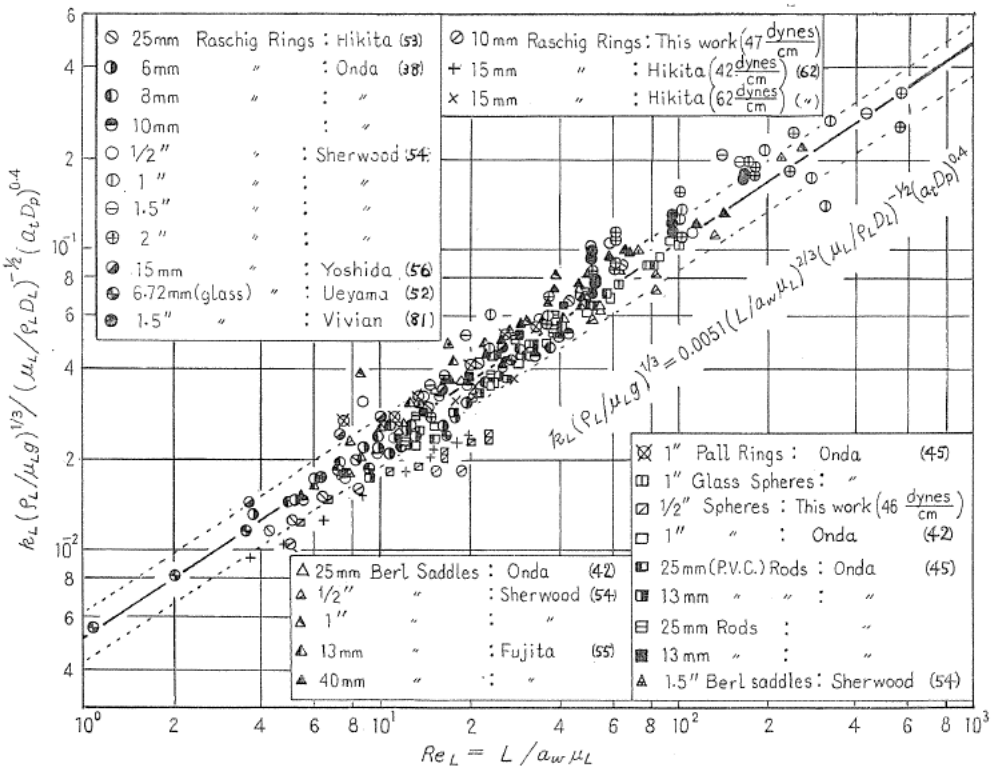

FIG. 37. Correlation of liquid-phase data for gas absorption and desorption.

Since the surface tension of surfactant solutions is smaller than water and a_w become larger, the liquid velocity on packing becomes essentially lower, so that k_L falls. This fact suggests that Eq. (60) is not applicable to the solution having smaller surface tension than water.

From these reasons, it is considered that a modified Reynolds number $L/a_w\mu$ replaced a_t in Re by a_w[46] rationally prescribes the flow condition on packings. Fig. 37 shows the plots of $k_L(\rho_L/\mu_L g)^{1/3}/(\mu_L/\rho_L D_L)^{-1/2}(a_t D_P)^{0.4}$ vs. $L/a_w\mu_L$, and a straight line represents

$$k_L\left(\frac{\rho_L}{\mu_L g}\right)^{1/3} = 0.0051\left(\frac{L}{a_w\mu_L}\right)^{2/3}\left(\frac{\mu_L}{\rho_L D_L}\right)^{-1/2}(a_t D_P)^{0.4} \qquad (61)$$

In Fig. 37, for the absorption of CO_2 into water added a surfactant, a non-foaming surfactant were used and the surface tensions of solutions were 47 dyn/cm. The values of k_La obtained are smaller than those of water as well as the literature data. As seen in Fig. 37, the k_L separated from these data with Eq. (57) deviate pretty from Eq. (61). This deviation may result from the reduction of liquid mixing at the junction of packing pieces as pointed out by Hikita[62] and the interfacial resistance with increase of surfactant concentration.

On the other hand, for the gas absorption by organic solvent in packed columns, there are so far only a few data. In our laboratory, the absorption of

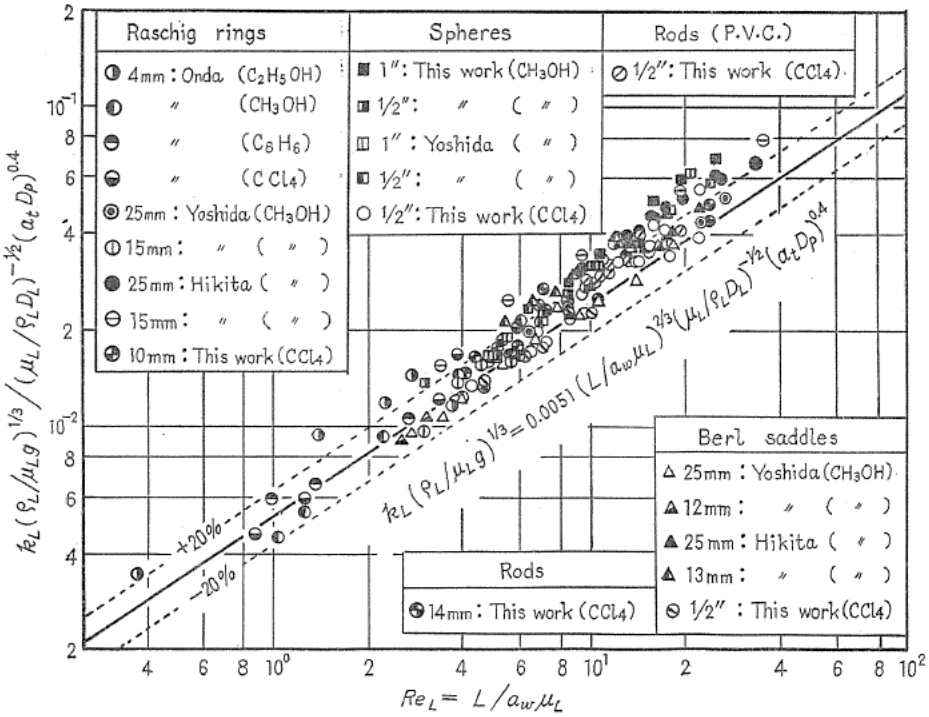

FIG. 38. Correlation of absorption data by using organic solvent with. Eq. (61).

pure CO_2 into metanol, ethanol, carbon tetrachloride and benzen were carried out in the column packed with Raschig rings Berl saddles, spheres and rods[40)46)]. Applying Eq. (57) to separate k_L from k_La data obtained and reported in the literature for organic solvents, the same plotting as Fig. 37 are shown in Fig. 38, in which the agreement between the observed value and Eq. (61) is also satisfactory.

Thus, the liquid phase mass transfer coefficients, k_L, for the gas absorption and desorption in packed columns have been correlated by Eq. (61) within an error of $\pm 20\%$ for organic solvents as well as water or aqueous solution.

6.2. Gas phase mass transfer coefficients: k_G

In numerous investigations of mass transfer in packed columns, empirical correlations on gas phase coefficients have not been so accurate as those on liquid phase one. Especially, the discrepancies are apparent when gas phase capacity coefficient are measured by two different methods, *i.e.* the vaporization of pure liquids into gases and the absorption of highly soluble gases into liquids from carrier gases.

Onda *et al.*[41)43)] obtained the k_G for Raschig rings, Berl saddles and spheres under the assumption that the effective surface area is equal to a_w, and k_G were correlated with

$$\frac{k_G RT}{a_t D_G} = 2.15\left(\frac{G}{a_t\mu_G}\right)^{0.8}\left(\frac{\rho_G^2 g}{\mu_G^2 a_t^3}\right)^{0.2}\left(\frac{\mu_G}{\rho_G D_G}\right)^{1/3}(a_t D_P)^{-3.0} \qquad (62)$$

where k_Ga data were obtained from the absorption of ammonia in nitrogen gases into water, and the exponent of 1/3 on the Schmidt number was assumed conventionally. However, as on the gravity force, g, in Eq. (62) the existence in continuous gas phase is doubtful and also Eq. (62) shows that the smaller packings gives lower k_G in opposition to those for nonirrigated packed beds, it was reexamined on the basis of Eq. (57).

The k_G divided from k_Ga data for gas absorption containing the literature values by a_w of Eq. (57) are shown in Fig. 39 as the plots of $(k_GRT/a_tD_G)/(\mu_G/\rho_GD_G)^{1/3}(a_tD_P)^{-2.0}$ vs. $G/a_t\mu_G$. The equation for the best line drawn through the data points in the higher group in Fig. 39 is as follows[46];

$$\frac{k_GRT}{a_tD_G}=5.23\left(\frac{G}{a_t\mu_G}\right)^{0.7}\left(\frac{\mu_G}{\rho_GD_G}\right)^{1/3}(a_tD_P)^{-2.0} \tag{63}$$

where the dependence of k_G on (a_tD_P) was obtained to be -2.0 approximately from the representative data of 1 in-Berl saddles and Raschig rings, but this dependence is not known for certain. In Fig. 39, the data points for Raschig rings and Berl saddles smaller than 15 mm are situated on the lower group,

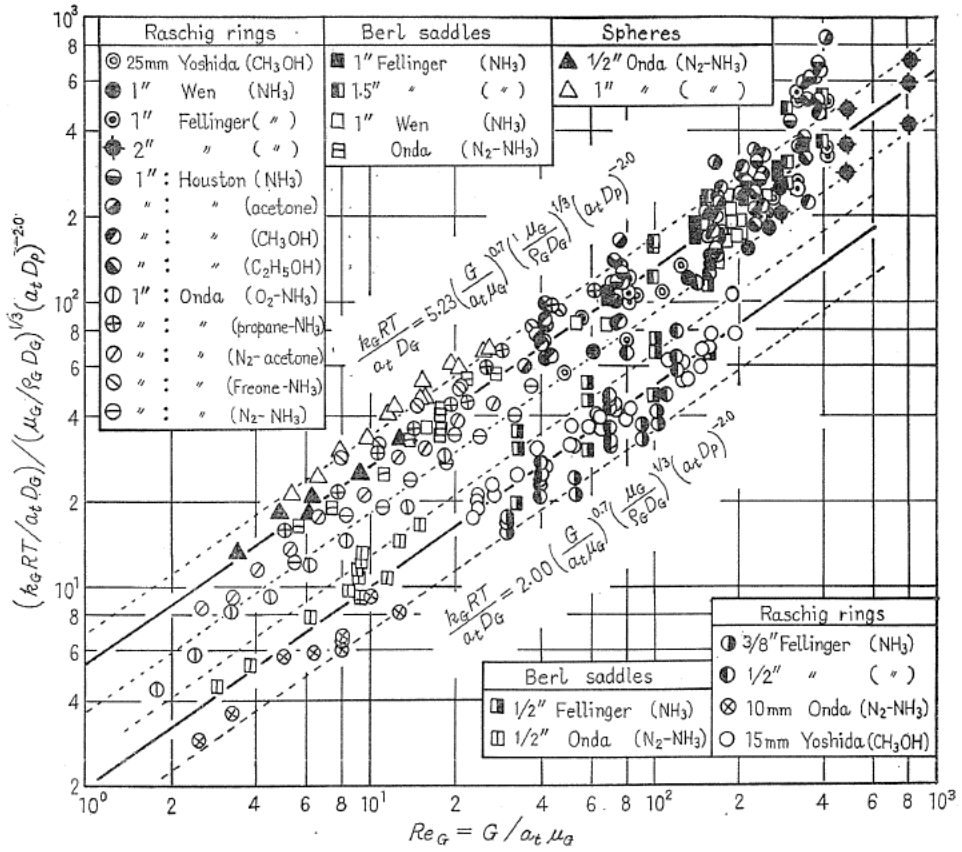

FIG. 39. Correlation of gas-phase data for gas absorption.

and are best correlated by merely changing the constant 5.23 in Eq. (63) into 2.00. This difference comes from the fact that k_Ga data for packing smaller than 15 mm tend to decrease monotonaously with an increase of a_t. However, this cause is not clear at present. The j_D-factor for mass transfer can be obtained by rearranging Eq. (63). For example, since for spheres $a_tD_P=6(1-\varepsilon)=3.4$, Eq. (63) becomes

$$j_D = 0.771\,[GD'_P/\mu_G(1-\varepsilon)]^{-0.30} \tag{64}$$

Shulman *et al.*[49] reported the following equation for saublimtion of dry naphtalene packings,

$$j_D = 1.195\,[GD'_P/\mu_G(1-\varepsilon)]^{-0.38} \tag{65}$$

where D'_P is the diameter of sphere possesing the same surface area as a piece of packing: ε is the void fraction of packed bed. The agreement between Eqs. (64) and (65) is fairly good within the region of $100<GD'_P/\mu_G(1-\varepsilon)<10{,}000$, as shown in Fig. 40.

Although in Eq. (63) the effect of diffusivity on the gas phase mass transfer coefficient was assumed to be $k_G \propto D_G^{2/3}$, it has been reported that the exponent of D_G for gas phase varies from 0.15 to 1.0, and also is not clear whether the diffusivity or Schmidt number is the pertinent variable. Recently, Vidwans-

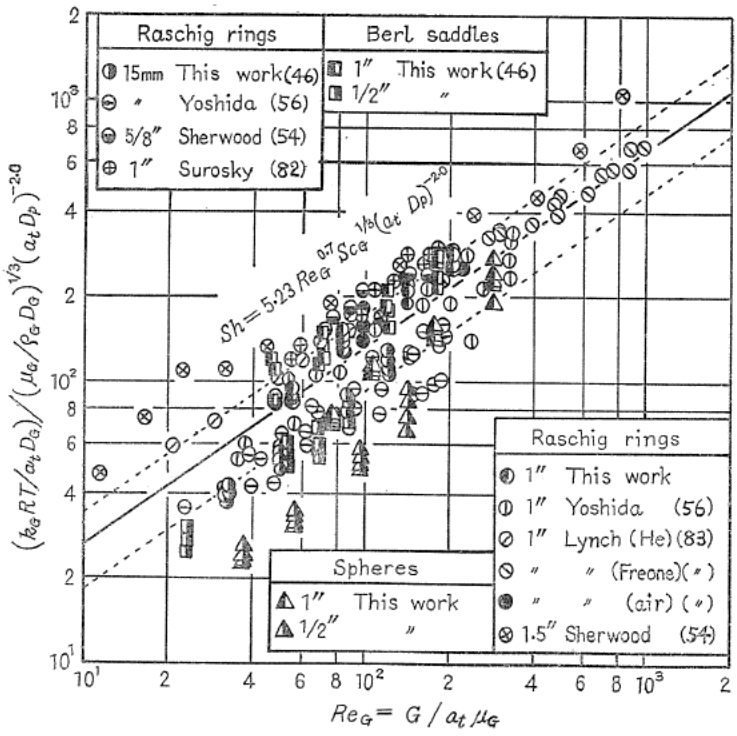

FIG. 40. Correlation of vaporization data with Eq. (63).

Sharma[57] have published that the diffusivity rather than the Schmidt number is the pertinent correlating factor and k_G is approximately proportional to $D_G^{1/2}$ at a given value of superficial gas velocity.

On the other hand, as mentioned above, it has been reported that the k_Ga obtained by water vaporization into air are higher than those obtained for gas absorption. However, there are considerable differences among the published data for vaporization because of the difficulties in experimental observation.

To ascertain their results, the rate of vaporization were measured for air-water system under adiabatic conditions, *i.e.* constant temperature of water[46]. To compare the k_Ga obtained for vaporization with those for gas absorption, k_Ga data were divided by a_w of Eq. (57), and the plots based on Eq. (63) are shown in Fig. 41. As seen in Fig. 41, Eq. (63) correlates almost all of the data for vaporization as well as gas absorption, but for 1/2 in-sphere the constant of Eq. (63) might be changed into 2.00.

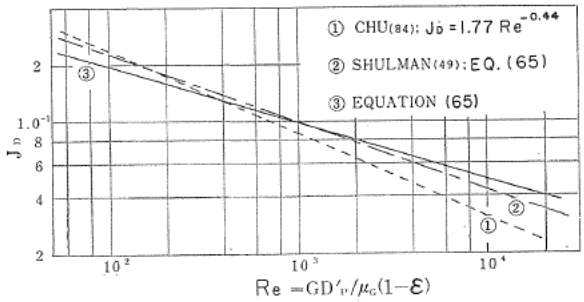

FIG. 41. Comparison of k_G-correlations by j_D-factor.

6.3. Applicability to distillation processes

On distillation processes in packed columns, it has been studied by many investigators. Actually, a distillation process is equimolar counter diffusion, while the gas absorption or vaporization is unidirectional, but this difference in both processes would have little effect on the individual mass transfer coefficients. In gas absorption, it is reasonable to obtain the average film coefficient in packed column, because the temperature and concentration of mixture differ greatly at each point through the column. Yoshida-Koyanagi[61] have discussed the applicability of H_G and H_L derived for gas absorption to the distillation in a packed column.

In our study[46], using the point values of k_G and k_L calculated from Eqs. (61) and (63) for gas absorption and gas-liquid interfacial area from Eq. (57), the height of packed column for distillation was calculated by

$$Z = G_M \int_{y_1}^{y_2} \left(\frac{1}{k_G a} + \frac{m}{k_L a \cdot C_{av}} \right) \frac{dy}{y^* - y} \tag{66}$$

in which the gas molar flow rate, G_M, is assumed to be constant through the column. Thus, the heights of packings calculated from Eq. (66) have been compared with the actual height of packing used to obtain the published data

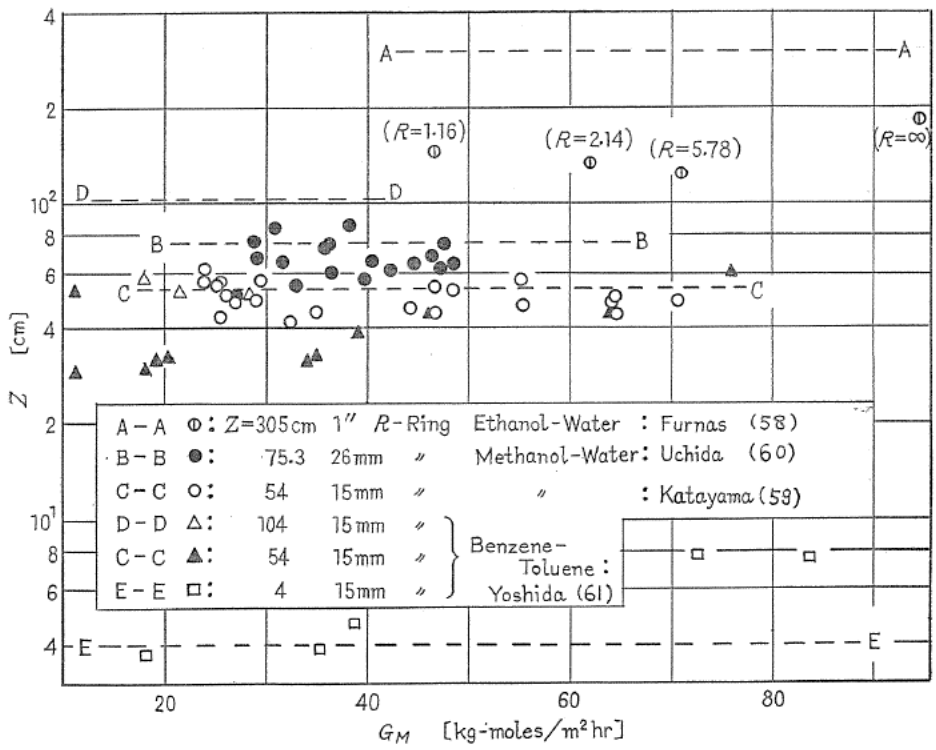

FIG. 42. Comparison of calculated and actual packed heights for distillation columns.

because the estimation of k_Ga or H_G used in the previous literature is insignigicant, especially for non-ideal mixtures.

The published data used for this calculation include the systems of benzen-toluene, methanol-water and ethanol-water at total or finite reflux ratio. Comparison of the caculated value, Z_{cal}, with the actual, Z_{act}, are shown in Fig. 42 against G_M. Their agreements are within $\pm 30\%$ except columns higher than 1.0 m, in which the maldistribution of liquid would occur.

The relative magnitude of individual phase resistance depends on the group mG/L, but the variable range in L/G is more restricted in distillation than in gas absorption. Furthermore, m and physical properties of liquid mixtures may vary widely from top to bottom throughout the column, and hence the relative magnitude of individual phase contributions depends on the liquid composition.

7. Gas Absorption with Chemical Reaction in Packed Column

A number of theoretical and experimental studies have been reported for gas absorption accompanied by chemical reaction, but for a packed column the theoretical treatment of such chemical reaction has been difficult. In general, the rate of gas absorption with chemical reaction can be expressed by

$$N_A^\circ = \beta k_L(C_{Ai} - C_{A0}) = k_L^\circ(C_{Ai} - C_{A0}) \tag{67}$$

where β is the so-called reaction factor; C_{A0} is the concentration of solute absorbed in the bulk of liquid and becomes zero for an irreversible reaction.

As described in Chap. 4.4, the reaction factor is presented for the simultaneous chemical reaction with first, second and generalized order, based on the particular models of the fluid dynamics of the process.

7.1. Absorption of CO_2 by aqueous sodium hydroxide in a packed column

The applicability of the film theory for gas absorption with a second order reaction to the absorption of CO_2 in aqueous sodium hydroxide solutions in a packed column may be confirmed by using Eq. (61) for k_L and Eq. (63) for k_G, under the assumption that the wetted surface area on packing is identical with the gas-liquid interface. The reaction between CO_2 and sodium hydroxide in aqueous solution takes place by Eqs. (33) and (34) as described in Chap. 4.1. Thus, the absorption mechanism is regarded as the gas absorption accompanied by a relatively slow second order reaction.

The overall capacity coefficients for the aqueous solutions of 0.05, 0.1, 0.25, 0.5 and 1.0 N-NaOH were observed in the column packed with 15 mm-Raschig rings, and those are plotted in Fig. 43 against the liquid flow rate, L.

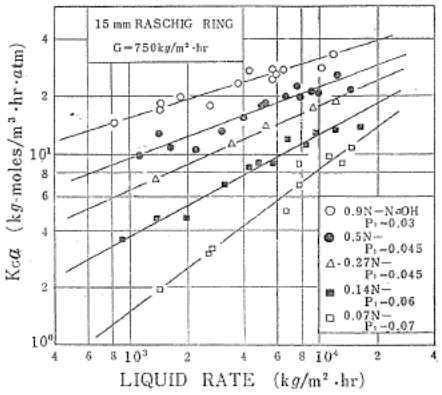

FIG. 43. K_Ga data for CO_2 absorption into aqueous NaOH solutions at 30°C.

The rate constant for Eq. (33) controlling the reaction between CO_2 and NaOH, is expressed from Fig. 14-b at 30°C as follows:

$$\log k_r = 3.875 + 0.133\, I \tag{68}$$

To estimate the diffusivity of CO_2 in aqueous sodium hydroxide solutions, the modified Stokes-Einstein's equation (41) was used. The ratio of D_{OH^-} to D_{CO_2} in sodium hydroxide solution, r, is 1.67 at 20°C according to Nijsing *et al.*[29], and so this value was used by assuming that r is independent of temperature ranging from 20 to 30°C. Saturated concentration of CO_2 in aqueous solution

TABLE 8. Liquid properties of NaOH solution, diffusivity, Henry's law constant and reaction rate constant of CO_2 in aqueous NaOH solutions at 30°C

$[OH^-]$	ρ(kg/m³)	μ(kg/m•hr)	σ(dyne/cm)	$D_L\times10^6$ (m²/hr)	$H\times10^2$ [kg-mol/m³•atm]	$k_r\times10^{-7}$ [m³/kg-mol•hr]
0.91	1037	3.49	72.5	6.62	2.26	3.57
0.51	1019	3.23	71.9	7.13	2.54	3.15
0.27	1009	3.07	71.6	7.49	2.71	2.93
0.14	1004	2.98	71.4	7.67	2.84	2.82
0.07	1001	2.93	71.3	7.81	2.91	2.76
0	996	2.88	71.2	7.92	2.97	2.59

was estimated by the van Krevelen's method, under the assumption that the salting-out effect of NaOH is the same as Na_2CO_3. Values of k_r, D_L and H estimated by the above mentioned methods and the physical properties of liquids used are shown in Table 8.

The theoretical reaction factor, β, for each experimental condition was calculated by

$$\beta = \gamma\sqrt{1-[(\beta-1)/rq]}/\tanh\gamma\sqrt{1-[(\beta-1)]/rq} \qquad (69)$$

where $\gamma = \sqrt{k_r C_B D_L}/k_L$, and the concentration of NaOH was calculated as a arithmetic mean value of inlet and outlet liquid concentration $\overline{C}_B$. As a result, the experimental conditions correspond to the region of a pseudo first order reaction as well as a slow second order reaction.

The observed values of β in the packed column can be determined from Eq. (70), assuming that the mass transfer resistances in each phase are additive

$$1/K_G a = 1/k_G a + 1/H\beta k_L a \qquad (70)$$

and using the individual capacity coefficients, $k_G a$ and $k_L a$, for physical absorption as the product of k_G calculated by Eq. (63) or k_L by Eq. (61) and a_w by Eq. (57). The predicted value of $k_G a$ amounted to about 10% of the total resistance for 1.0 N solution, but in the dilute sulution it was less than a few per cent. The values of β_{obs} obtained by Eq. (70) are compared with β_{theo} calculated by Eq. (69) in Fig. 44. The observed and theoretical values of β are in agreement within an error of $\pm 30\%$.

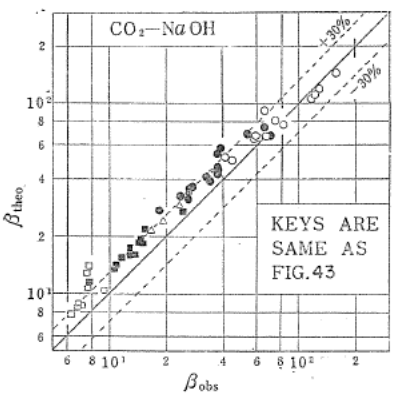

FIG. 44. Theoretical and observed values of β for CO_2 absorption into aqueous NaOH solutions.

On the other hand, in the case of a pseudo first order reaction it is possible to obtain the interfacial area in the packed column, when the value of γ is greater than 3

$$a = k_L^\circ a/\beta k_L = k_L^\circ a/\sqrt{k_r \overline{C}_B D_L} = k_L^\circ a/\sqrt{k' D_L} \qquad (71)$$

where $k_r\overline{C}_B$ represents the pseudo first order reaction rate constant and is identical to k'.

The effective surface areas, a, were calculated by Eq. (71) from $K_G a$ or $k_L^\circ a$ data reported in the literature on the chemical absorption. Fig. 45 shows a for Raschig ring with a line of a_w by Eq. (57) and a dotted line of a_w by Hikita's correlation[47]. The agreement between a_w and a shows that the gas-liquid interface is uniformly effective and essentially identical with wetted surface for gas absorption with a pseudo first order reaction. Also, for Berl saddles and spheres, the effective surface areas calculated from $K_G a$ data on CO_2-NaOH system agree well with a_w by Eq. (57).

Furthermore, as seen in Fig. 44, the agreement between β_{theo} and β_{obs} for a second order reaction within a reasonable error substantiates the assumption

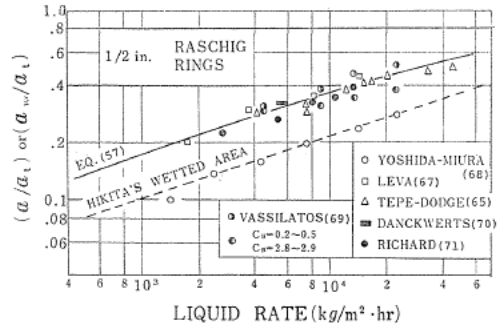

FIG. 45. Interfacial areas for chemical absorption and wetted surface area in packed columns.

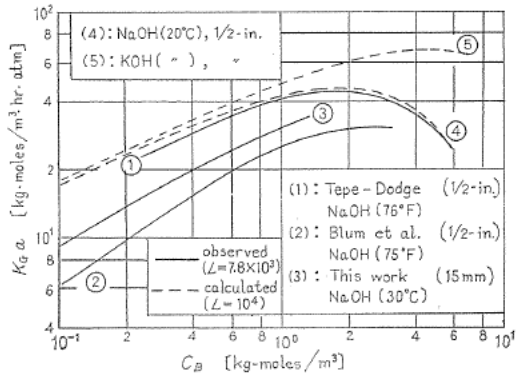

FIG. 46. Effect of alkali concentration on rate of absorption of CO_2.

that $a=a_w$ may be applicable for the chemical absorption in packed columns.

The effect of alkali concentration on K_Ga has been discussed[63)64)]. In Fig. 46, the data of Tepe-Dodge[65)] shows the maximum point of K_Ga at about 1.8 N-NaOH. Such a relation is seemed to be originated in changes of the diffusivity and solubility of solute gas in electrolyte solution. Assuming a pseudo first order reaction, K_Ga for alkaline solution would be calculated from Eqs. (70) and (71). As a result, as shown in Fig. 46, the values of K_Ga calculated for the absorption of CO_2 in NaOH solution agree well with the observed value and shows a maximum point at 1.75 N. For KOH solutions, the calculated K_Ga is shown by a curve 5 in Fig. 46, and the maximum K_Ga may be found at about 4.5 N. This difference in C_B between NaOH and KOH solutions comes from the fact that a variation of the viscosity of KOH solution with C_B is smaller than one of NaOH solutions.

7.2. Gas absorption with chemical reaction in packed column under adiabatic conditions[72)]

The absorption of pure carbon dioxide or pure sulfur dioxide by sodium hydroxide solutions in a packed column under adiabatic conditions was discussed. Furthermore, the effect of the heat of solution on the absorption rate of gas

were also investigated. No effect of inlet gas temperature on gas absorption rate was observed. However, the liquid concentration and temperature, respectively, varied markedly throughout the column. The difference in concentration of sodium hydroxide at the top and bottom of the column is plotted against that of temperature in Fig. 47. The straight lines in Fig. 47 represent the thermal equation

$$T_t - T_0 = (C_{B0} - C_{Bt})(-\Delta H_S - \Delta H_R)/C_P\rho \tag{72}$$

where T_t and T_0 are the temperature of liquid at the top and bottom of the column, respectively: C_{Bt} and C_{B0} are the concentration of NaOH at the top and bottom, respectively: ΔH_S is the heat of solution: ΔH_R is the heat of reaction: C_P is the specific heat of liquid: ρ is the liquid density.

Based on the assumption that the liquid flow is piston-like, the material balance for any differential column height, dz, leads to

$$u\frac{dC_B}{dz} = -\frac{\beta k_L a}{H} = -\frac{uV\beta k_L a C_{Ai}}{Fz_t} \tag{73}$$

with boundary conditions

$$\begin{aligned} C_B &= C_{B0} \quad \text{at} \quad z = 0 \\ C_B &= C_{Bt} \quad \text{at} \quad z = z_t \end{aligned} \tag{74}$$

where u is the superficial liquid velocity in the column: V is the volume of the column. Eq. (73) is changed to dimensionless form by substituting $Y = C_B/C_{B0}$ and $Z = z/z_t$, and then integrating with boundary condition (74) to give

$$\frac{FC_{B0}}{V}\int_{Y_t}^{1.0}\frac{dY}{\beta k_L a C_{Ai}} = \frac{FC_{B0}}{V}\int_{Y_t}^{1.0}\frac{dY}{\beta N_A} \tag{75}$$

where F is the volumetric flow rate of liquid: N_A is the physical absorption rate defined by $k_L a C_{Ai}$. Values of β and N_A in Eq. (75) vary with the packed height because liquid temperature and concentra-

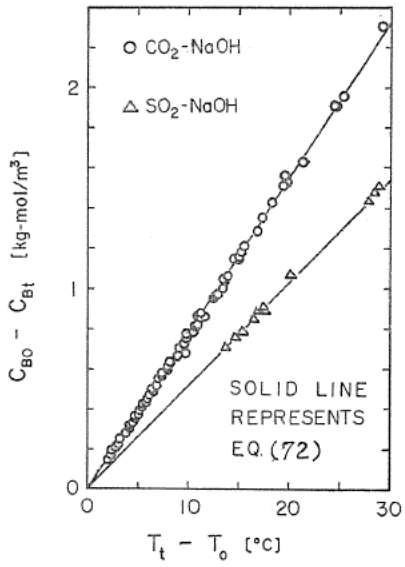

FIG. 47. Relation between the difference of concentration of NaOH and that of liquid temperature through a packed column.

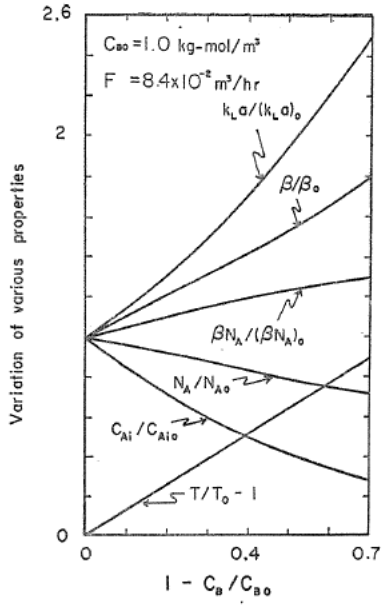

FIG. 48. Variations of physicochemical properties in a packed column for SO_2-NaOH system.

tion of NaOH vary in the column. Thus, Eq. (75) must be integrated graphically. Then the liquid temperature was calculated from Fig. 47. The temperature of gas-liquid interface was estimated by the method of Kobayashi-Saito[74]. Values of k_L, a and C_{Ai} were evaluated from Eq. (60), (57) and (11), respectively.

Fig. 48 shows the variations of k_La, T, etc. for SO_2-NaOH system calculated from the methods above mentioned. The variation of the product of β and N_A is smaller than that of other physicochemical properties. Consequently, the product of β and N_A is may be assumed to be constant throughout the column, and can be calculated based on the mean values of temperature and concentration at the inlet and the outlet of the column. As a result, Eq. (75) becomes

$$\beta = FC_{B0}(1 - Y_t)/(VN_A) \tag{76}$$

In Fig. 49, the values of β obtained from Eq. (76) are plotted against the theoretical ones estimated from the film theory. In the calculation of the theoretical value of β, the reaction between carbon dioxide and sodium hydroxide is considered to be an irreversible second order reaction. The reaction between sulfur dioxide and sodium hydroxide is considered to be a two-step consecutive instantaneous chemical reaction as given by Onda *et al.*[73] or Hikita[75], and reaction factor is evaluated by

$$\beta = 1 + \frac{r_F}{2}\left(1 + \frac{r_{P1}}{r_{P2}}\right)\left(\frac{C_{FL}}{C_{Ai}}\right) + r_{P1}\left(\frac{C_{PL}}{C_{Ai}}\right) \tag{77}$$

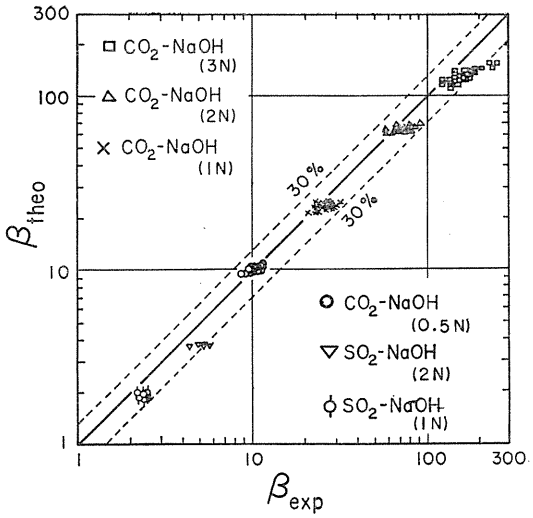

Concentration in parentheses shows the initial values of sodium hydroxide.
Experimental conditions:
$z_t = 0.07 \sim 0.4$ m, $C_{B0} = 0.5 \sim 3.0$ kg-mol/m^3
$F = 1.8 \times 10^{-2} \sim 11.1 \times 10^{-2}$ m^3/hr
conversion of sodium hydroxide = 9~22%

FIG. 49. Comparison of the theoretical and experimental values.

where

$$r_E = [12/(6+Q+K)](D_E^*/D_A)$$

$$r_{P1} = \{[-(1+3D_F^*/D_P^*) + \sqrt{1+24D_F^*/D_P^*}]/(2-D_F^*/D_P^*)\}(D_P^*/D_A)$$

$$r_{P2} = \{9/[3+(Q+K)D_P^*/D_E^*]\}(D_P^*/D_A)$$

$$K = \sqrt{(6-Q)^2 + 24(D_E^*/D_P^* - 1)Q}$$

$$Q = C_{FL}/C_{CL}$$

and D_i^* is the ionic self-diffusivity, indicating the i-species: subscripts C, E and F are the sodium, hydroxide, and bisulfite ions, respectively. As shown Fig. 49, observed values of β are in good agreement with theoretical values within an error of $\pm 30\%$. Thus the overall reaction factor in a packed column can be evaluated from Eq. (76) by using the mean values of temperature and concentration at the top and bottom of the column, respectively.

7.3. Absorption of oxygen into sodium sulphite solutions in a packed column[77]

The absorption of oxygen into sodium sulphite solutions in packed columns has been studied to determined the interfacial areas by several investigators. On the reaction kinetics of dissolved oxygen with sulphite ion, Onda *et al.*[22] have obtained such a result as described in Chap. 4.3. However, according to the recent paper[79], the reaction order for oxygen depends on the oxygen concentration in the liquid phase at the interface.

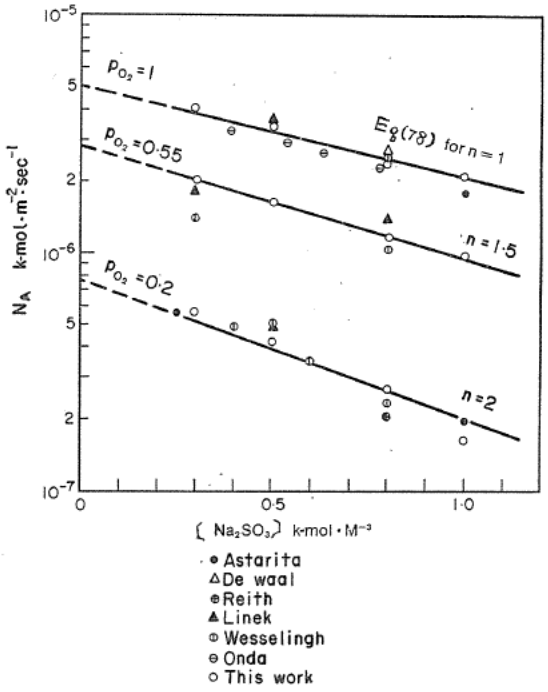

FIG. 50. Effect of sulphite concentration on the absorption rate. $C_{CoSO_4}=10^{-3}$, pH=8.0.

To investigate the influence of oxygen pressure upon the absorption rate and the interfacial area in packed columns, the absorption of oxygen by sodium sulphite solutions in the presence of cobalt sulphate as a catalyst was carried out in the column packed with 15 mm Raschig rings.

For a pseudo n-th order reaction, the relation between the absorption rate of oxygen and the concentration of sulphite solution is given by Eq. (78) with salting-out parameter K_S as well as Eq. (43)

$$\log N_A = \log\left(\frac{2}{n+1} D_A k_n C_{Ai}^{n+1}\right)^{1/2} - \frac{3(n+1)}{2} K_S C_{Na_2SO_3} \tag{78}$$

When the variation of D_A is small for the concentration change of sulphite solution and the reaction rate constant, k_n, is constant, it will be found that there is a linear relation between log N_A and $C_{Na_2SO_3}$. Fig. 50 shows our data and literature data. The model of $n=1$ is suitable for $P_{O_2}=1$, of $n=1.5$ for $P_{O_2}=0.55$, and of $n=2$ for $P_{O_2}=0.2$ as shown in Fig. 50. Furthermore, the absorption rate of oxygen are plotted against the partial pressure of oxygen P_{O_2} in Fig. 51, and the reaction order for oxygen varies gradually from the second to the first order with increase of P_{O_2}.

On the other hand, with the surface renewal model of Danckwerts the rate of gas absortion with a rapid first order reaction is given by

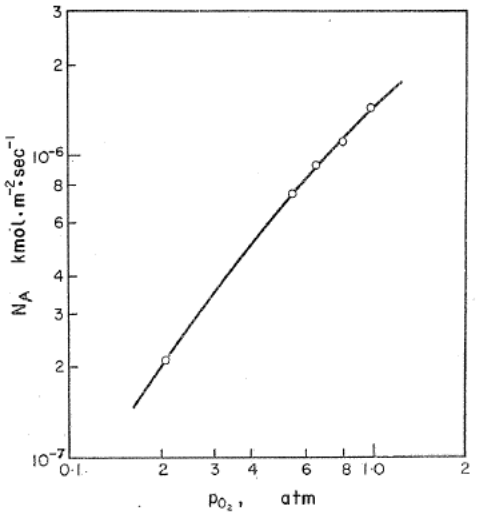

FIG. 51. Effect of the oxygen pressure on the absorption rate. $C_{Na_2SO_3}=0.5$, $C_{CoSO_4}=10^{-4}$, pH=8.5.

$$N'_A = C_{Ai}\, asz\sqrt{(k_1+s)D_A} \tag{79}$$

When $(N'_A/C_{Ai})^2$ is plotted against k_1, the slope of this line yields the interfacial area, a, and the intersection of the line with the abscissa give the surface renewal rate, s.

For the gas absorption with a pseudo first order reaction, the value of a can be calculated by Eq. (71). The reaction rate constant, k_1, is interpolated from the data given by de Waal *et al.*[78] and the influences of $C_{Na_2SO_3}$, C_{CoSO_4}, pH and T upon k_1 are determined by Eq. (45).

The interfacial areas estimated from Eqs. (79) and (71) are shown in Fig. 52 in which a/a_t is plotted against the liquid flow rate, and agree well with value of a_w obtained by Eq. (57), while the results by de Waal[77] do not agree with our correlation. This disagreement comes from the fact that the data obtained by using air as gas in their experiments were applied to the surface renewal model of Danckwerts. It was found that the interfacial area observed by using pure oxygen are about 1.5 times higher than those using air. Therefore, the

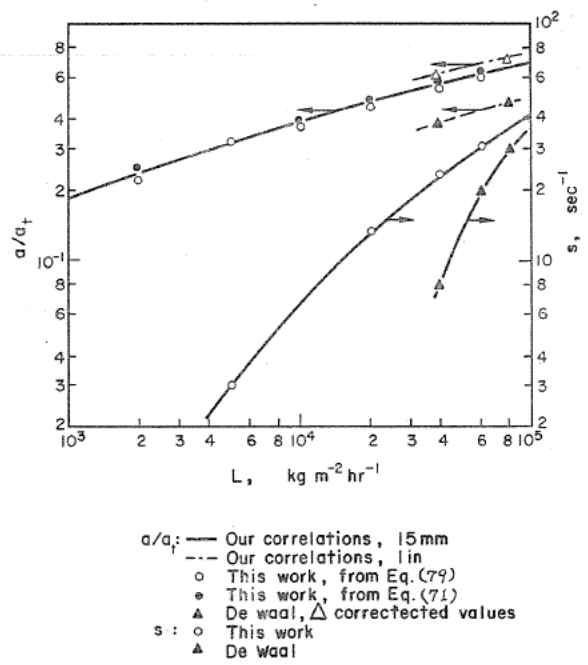

FIG. 52. Effect of the liquid flow rate on the interfacial areas and the surface renewal rate. $P_{O_2}=1$.

literature's values of the interfacial areas observed by using air for the oxidation of sulphite solutions in various absorption devices must be corrected. If the interfacial areas obtained by de Waal are corrected, their values agree well with our correlations as shown in Fig. 52. From this result, it is found that our correlations, Eq. (57), (61), and (63) would be applicable to large packed columns.

8. Conclusion

Packed column is the most simple device in the chemical industry. Nevertheless, many knowledges in Equilibria, Physicochemical Properties, Reaction Kinetics, Effective Surface Area, and Mass Transfer Coefficients are necessary to design it accurately. This paper contains many data or correlations in each field which were investigated in our laboratory during about 20 years. I believe these results would be very usefull to design not only packed columns but also other absorption equipments.

Acknowledgment

I express my heartily gratitude to Assistant Professor Dr. Hiroshi Takeuchi for his arrangement on our many investigations and to Miss Mieko Hasegawa for the type-writing of this paper.

Literature cited

1) Onda, K., S. Aiso and H. Suzuki: Memoirs of the Faculty of Engineering, Nagoya University, **IV-2**, 118 (1951).
2) Onda, K. and M. Murayama: Kogyo-Kagaku-Zasshi, **56**, 731 (1953).
3) Onda, K. and M. Murayama, F. Otsubo and H.Kitazawa: *ibid.*, **57**, 731 (1954).
4) Onda, K. and S. Dooke: Nenryo-Kyokai-Shi, **34**, 418 (1955).
5) Miyagawa, I., K. Onda and E. Sada: Kagaku Kogaku, **20**, 671 (1956).
6) Onda, K., E. Sada and Y. Jinno: Kogyo-Kagaku-Zasshi, **61**, 702 (1958).
7) Onda, K., E. Sada, T. Kobayashi, S. Kito and K. Ito: J. of Chem. Eng. Japan, **3**, 18 (1970).
8) Onda, K., E. Sada, T. Kobayashi, S. Kito and K. Ito: *ibid.*, **3**, 137 (1970).
9) Van Krevelen, D. W. and P. J. Hoftijzer: Chem. Ind. XXIeme Congr. Int. Chem. Ind., 168 (1948).
10) Onda, K., H. Mori and S. Oda: Kogyo-Kagaku-Zasshi, **63**, 116 (1960).
11) Onda, K., T. Okamoto and Y. Yamaji: Kagaku Kogaku, **24**, 918 (1960).
12) Othmer, D. F. and M. S. Thakar: Ind. Eng. Chem., **45**, 589 (1953).
13) Wilke, C. R., and P. Chang: A. I. Ch. E. Journal, **1**, 264 (1955).
14) Onda, K., H. Takeuchi and Y. Okada: Preprint of 5-th General Symp. of Chem. Engrs. of Japan (Osaka), p. 3 (1966).
15) Onda, K., E. Sada, T. Kobayashi, N. Ando and S. Kito: Kagaku Kogaku, **34**, 603 (1970).
16) Gubbins, K. E. *et al.*: A. I. Ch. E. Journal, **12**, 584 (1966).
17) Ratcliff, G. A. and J. G. Holdcroft: Trans. Inst. Chem. E,ngrs., **41**, 315 (1963).
18) Onda, K., H. Takeuchi, T. Kobayashi, M. Takahashi and M. Fujine: Kagaku Kogaku, **36**, 903 (1972).
19) Jones, G. and M. Dole: J. Am. Chem. Soc., **51**, 2950 (1929).
20) Onda, K., E. Sada and Y. Miwa: Preprint of 10th Kenkyu-Danwa-Kai of Chem. Engrs. (Nagoya), p. 1 (1964).
21) Onda, K., T. Kobayashi and T. Nagase: Kogyo-Kagaku-Zasshi, **70**, 1271 (1967).
22) Onda, K., E. Sada, T. Kobayashi and M. Fujine: Kagaku Kogaku, **34**, 187 (1970).
23) Onda, K., E. Sada, T. Kobayashi and M. Fujine: Chem. Eng. Sci., **25**, 753 (1970).
24) Onda, K., E. Sada, T. Kobayashi and M. Fujine: *ibid.*, **25**, 761 (1970).
25) Onda, K., E. Sada, T. Kobayashi and M. Fujine: *ibid.*, **25**, 1023 (1970).
26) Onda, K., E. Sada, T. Kobayashi and M. Fujine: *ibid.*, **27**, 247 (1972).
27) Danckwerts, P. V.: Trans. Faraday Soc., **46**, 300 (1950).
28) Moelwyn-Hughes: "The Kinetics Reaction in Solution", p. 120 (1947).
29) Nijsing, R. A. T. O., R. H. Hendriksz and H. Kramers: Chem. Eng. Sci., **10**, 88 (1959).
30) Pinsent, B. W., L. Person and F. J. W. Roughton: Trans. Faraday Soc., 52, 263 (1956).
31) Yagi, S. and H. Inoue: Chem, Eng. Sci., **17**, 411 (1962).
32) De Waal, K. J. A. and J. C. Okeson: Chem. Eng. Sci., **21**, 559 (1966).
33) Srivastava, R. D., A. F. McMillan and I. J. Harris: Can. J. Chem. Eng., **46**, 181 (1968).
34) Hatta, S.: Tech. Repts. Tohoku. Imp. Univ., **8**, 1 (1928), **10**, 119 (1932).
35) Hikita, S. and S. Asai: Kagaku Kogaku, **27**, 823 (1963).
36) Onda, K., T. Kobayashi and M. Fujine: Kogyo-Kagaku-Zasshi, **74**, 547 (1971).
37) Onda, K., T. Kobayashi, M. Fujine and M. Takahashi: Chem. Eng. Sci., **26**, 2009 (1971).
38) Onda, K., E. Sada and F. Otsubo: Kagaku Kogaku, **22**, 194 (1958).
39) Onda, K., E. Sada and I. Murase: A. I. Ch. E. Journal, **5**, 235 (1959).
40) Onda, K. and E. Sada: Kagaku Kogaku, **23**, 220 (1959).
41) Onda, K., E. Sada and M. Saito: *ibid.*, **25**, 820 (1961).
42) Onda, K., T. Okamoto and H. Honda: *ibid.*, **24**, 490 (1960).
43) Onda, K., E. Sada, C. Kido and A. Tanaka: *ibid.*, **27**, 140 (1963).
44) Onda, K., E. Sada, C. Kido and O. Kawatake: *ibid.*, **30**, 226 (1966).
45) Onda, K., H. Takeuchi and Y. Koyama: *ibid.*, **31**, 126 (1967).
46) Onda, K., H. Takeuchi and Y. Okumoto: J. of Chem. Eng. Japan, **1**, 56 (1968).

47) Hikita, H. and K. Kataoka: Kagaku-Kogaku, **20**, 528 (1956).
48) Weisman, J. and C. F. Bonilla: Ind. Eng. Chem., **42**, 1099 (1950).
49) Shulman, H. L., C. F. Ullrich, A. Z. Proulx and J. O. Zimmerman: A. I. Ch. E. Journal, **1**, 253 (1955).
50) Hikita, H.: Preprint of 3rd Symposium on Chem. Eng., Nagoya, Japan, p. 23 (1964).
51) Ellison, A. H. and W. A. Zisman: J. Phys. Chem., **58**, 260 (1954).
52) Ueyama, K., H. Hikita, S. Nishigami and S. Funahashi: Kagaku Kogaku, **18**, 68 (1954).
53) Hikita, H. and K. Kamo: *ibid.*, **18**, 454 (1954).
54) Sherwood, T. K. and F. A. L. Holloway: Trans. Am. Inst. Chem. Engrs., **36**, 39 (1940).
55) Fujita, S. and T. Hayakawa: Kagaku Kogaku, **20**, 113 (1956).
56) Yoshida, F. and T. Koyanagi: A. I. Ch. E. Journal, **8**, 309 (1962).
57) Vidwans, A. D. and M. M. Sharma: Chem. Eng. Sci., **22**, 673 (1967).
58) Furnas, C. C. and M. L. Taylor: Trans. Am. Inst. Chem. Engrs., **36**, 135 (1940).
59) Katayama, S., T. Koyanagi and F. Yoshida: Kagaku Kogaku, **22**, 764 (1958).
60) Uchida, S. *et al.*: *ibid.*, **11**, 53 (1947).
61) Yoshida, F. and T. Koyanagi: Ind. Eng. Chem., **46**, 1756 (1954).
62) Hikita, H.: Kagaku Kogaku, **24**, 9 (1960).
63) Onda, K., E. Sada and H. Takeuchi: J. of Chem. Eng. Japan, **1**, 62 (1968).
64) Onda, K. and H. Takeuchi: Preprint of 6th Chem. Reaction Kinetics Symposium of the Society of Chem. Engrs. (Nagoya), p. 151 (1966).
65) Tepe, J. B. and B. F. Dodge: Trans. Am. Inst. Chem. Engrs., **39**, 255 (1943).
66) Blum, H. A., L. F. Stutzman and W. S. Dodds: Ind Eng. Chem., **44**, 2969 (1952).
67) Leva, M.: A. I. Ch. E. Journal, **1**, 224 (1955).
68) Yoshida, F. and Y. Miura: *ibid.*, **9**, 331 (1963).
69) Vassilatos, G., O. Trass and A. I. Johnson: Can. J. Chem. Eng., **41**, 7 (1963).
70) Danckwerts, P. V., A. M. Kennedy and D. Roberts: Chem. Eng. Sci., **18**, 63 (1963).
71) Richards, G. M., G. A. Ratcliff and P. V. Danckwerts: *ibid.*, **19**, 325 (1964).
72) Onda, K., T. Kobayashi, S. Kato and H. Takeuchi: J. of Chem. Eng. Japan, **4**, 193 (1971).
73) Onda, K., T. Kobayashi and M. Odaka: Kagaku Kogaku, **33**, 886 (1969).
74) Kobayashi, T. and H. Saito: *ibid*, **29**, 512 (1965).
75) Hikita, H., S. Asai and A. Tsuji: Preprint of 34th Annual Meeting of the Society of Chem. Engrs., p. 64 (1969).
76) Van Krevelen, D. W. and P. J. Hoftijzer: Rec Tray. Chim., **67**, 563, 587 (1948).
77) Onda, K., H. Takeuchi and Y. Maeda: Chem. Eng. Sci., **27**, 449 (1972).
78) De Waal, K. J. A. and W. J. Beek: *ibid.*, **22**, 585 (1967).
79) Linek, V. and J. Mayrthoferova: *ibid.*, **25**, 787 (1970).
80) Danckwerts, P. V.: Ind. Eng. Chem., **43**, 1460 (1951).
81) Vivian, J. E. and C. J. King: A. I. Ch. E. Journal, **10**, 221 (1964).
82) Surosky, A. E. and B .F. Dodge: Ind. Eng. Chem., **42**, 1112 (1950).
83) Lynch, E. J. and C. R. Wilke: A. I. Ch. E. Journal, **1**, 9 (1955).
84) Chu, J. C., J. Kalil and W. A. Wetteroth: Chem. Eng. Progrs., **49**, 141 (1953).